Tissue-resident CD4$^+$ T helper cells assist protective respiratory mucosal B and CD8$^+$ T cell memory responses

Young Min Son[1,2], In Su Cheon[1,2], Yue Wu[1,2], Chaofan Li[1,2], Zheng Wang[1,2], Yao Chen[3], Yoshimasa Takahashi[4], Alexander L. Dent[5], Mark H Kaplan[5], Yang-Xin Fu[6], Justin J. Taylor[7], Weiguo Cui[3,8] and Jie Sun[1,2] *

1. Department of Medicine, Mayo Clinic, Rochester, MN 55905, USA
2. Department of Immunology, Mayo Clinic, Rochester, MN 55905, USA
3. Versiti Blood Research Institute, Milwaukee, WI 53213, USA
4. Department of Immunology, National Institute of Infectious Diseases, Shinjuku-ku, Tokyo 162-8640, Japan
5. Department of Microbiology and Immunology, Indiana University School of Medicine, Indianapolis, IN 46202, USA
6. Department of Pathology, UT Southwestern Medical Center, Dallas, TX, 75235, USA.
7. Vaccine and Infectious Disease Division, Fred Hutchinson Cancer Research Center, Seattle, WA, USA.
8. Department of Microbiology and Immunology, Medical College of Wisconsin, Milwaukee, WI 53226, USA

* Correspondence author. Email: sun.jie@mayo.edu

Abstract

The roles of $CD4^+$ T helper cells (T_H) in shaping localized memory B and $CD8^+$ T cell immunity in the mucosal tissues are largely unexplored. Here, we report that lung T_H cells provide local assistance for the optimal development of tissue-resident memory B (B_{RM}) and $CD8^+$ T (T_{RM}) cells following the resolution of primary influenza virus infection. We identify a population of tissue-resident $CD4^+$ T_H (*aka* T_{RH}) cells that co-exhibit follicular T helper (T_{FH}) and T_{RM} cell features and mediate local help of $CD4^+$ T cells to B and $CD8^+$ T cells. Optimal T_{RH} cell formation requires lung B cells and transcription factors involved in T_{FH} or T_{RM} development. Further, we show that T_{RH} cells deliver local help to B and CD8 T cells through CD40L and IL-21-dependent mechanisms. Our data have uncovered a new tissue-resident T_H cell population that is specialized in assisting the development of mucosal protective B and $CD8^+$ T cell responses *in situ*.

Introduction

The long-term protection against pathogen reinfection is mediated by long-lived plasma cells, memory B cells (B_{MEM}) and/or memory T (T_{MEM}) cells. In addition to circulating B_{MEM} and T_{MEM} cells, tissue-resident memory B (B_{RM}) and T (T_{RM}) cells that reside in the mucosal sites have recently been identified and characterized [1, 2, 3, 4, 5]. B_{RM} and T_{RM} cells are able to mount rapid recall responses *in situ* against invading pathogens before pathogen dissemination, and therefore are thought to provide immediate and superior protection against secondary infections [1, 6, 7, 8]. However, the mechanisms underlying the development and persistence of robust B_{RM} and T_{RM} cell responses in the respiratory tract are largely undefined. Furthermore, we do not know whether there are cellular and molecular pathways that can be targeted to simultaneously promote both B_{RM} and T_{RM} responses for maximal protection against pathogen reinfections.

Influenza viruses remain a leading cause of respiratory tract infections despite progress in antiviral therapies. Each year, influenza virus infects 5–10% of adults and 20–30% of children worldwide [9, 10], resulting up to 35.6 million illnesses and 56,000 deaths annually in the U.S. since 2010 [11]. Influenza virus infection induces potent development of protective B_{RM} and $CD8^+$ T_{RM} responses in the respiratory mucosal tissue [5, 12, 13]. Compared to B_{MEM} cells in the secondary lymphoid organs, lung B_{RM} have enhanced percentages of cells poised for cross-reactive memory repertoires, potentially due to the local supply of B_{RM} precursors by persistent germinal center (GC) responses in the inducible bronchus-associated lymphoid tissues (iBALT) following primary influenza infection [14]. Therefore, influenza-specific B_{RM} cells are thought to provide better cross-protection at the site of infection compared to their counterparts in the secondary lymphoid organs [1, 14]. Additionally, lung B_{RM} cells, but not systemic B_{MEM} cells, contributed to early plasmablast responses following influenza re-infection, which are potentially important in restricting early viral dissemination [1, 5, 14]. T_{MEM} responses against conserved influenza internal epitopes confer cross-reactive protection against influenza viruses that escape neutralizing antibody (Ab) responses [15, 16, 17, 18, 19, 20]. In animal models, influenza-specific lung $CD8^+$ T_{RM} cells can rapidly respond to heterologous influenza virus reinfection before it can replicate to high titers [21, 22]. Influenza-specific $CD8^+$ T_{RM} cells have also been detected in human lungs and are thought to be important for the protection against severe influenza-associated diseases [23, 24]. However, compared to other tissues, lung protective $CD8^+$ T_{RM} responses are short-lived in

nature [25, 26]. Thus, understanding the cellular and molecular mechanisms regulating the development and/or maintenance of lung protective B_{RM} and/or $CD8^+$ T_{RM} responses may aid the design of future influenza vaccines.

$CD4^+$ T helper (T_H) cells are important in anti-influenza immune responses by providing essential "help" for the development of effector and memory $CD8^+$ T and germinal center B (B_{GC}) cell responses [15]. $CD4^+$ T cells are not required for the generation of effector $CD8^+$ T cells during primary influenza infection [27], but are needed for the production of IL-10 by influenza-specific effector CD8 T cells [28]. $CD4^+$ T cell help, particularly during the priming stage, is vital for the development of circulating T_{MEM} and $CD103^+$ T_{RM} following primary influenza infection [29, 30]. Similarly, $CD4^+$ T cell help, mediated mainly through follicular helper T cells (T_{FH}) in the secondary lymphoid organs, is required for assisting B cells to form GC and the production of high affinity antibodies during influenza infection [31, 32, 33]. However, whether $CD4^+$ T cells can assist local B and $CD8^+$ T cell memory responses at the mucosal tissue following the resolution of primary infection is unknown. Several recent studies have also identified a population of PD-1^{hi} "T_{FH}-like" cells in the peripheral tissues during autoimmunity [34, 35, 36]. However, the developmental cues and the precise physiological functions of these cells remain largely elusive. During influenza infection, the existence of a lung "T_{FH}-like" cell population that can potentially sustain lung B_{GC} responses has been recently demonstrated [35, 37, 38], but is still controversial [5, 36].

Here, we have identified a population of lung $CD4^+$ helper T (T_H) cells developed after influenza viral clearance, co-exhibiting T_{FH} and T_{RM} features. Based on their gene expression, sessile features and functional properties, we termed these cells tissue-resident T helper cells (T_{RH}). Importantly, T_{RH} cells provide local help for the generation of strong B_{GC} and B_{RM} responses, as well as a $CD8^+$ T_{RM} population that is critical for the protection against heterologous influenza virus infection [39, 40]. We further identified the molecular cues mediating T_{RH} cell help to B and $CD8^+$ T cells. Our findings reveal a previously unidentified tissue-resident T_H cell population that is important in assisting local development of protective memory B and $CD8^+$ T cell responses in the respiratory mucosal tissue.

Results

Lung CD4$^+$ T cells provide "late" help for the formation of B_{GC}, B_{RM} and CD8$^+$ T_{RM} responses *in situ*

We sought to determine whether CD4$^+$ T cell help can assist local B and CD8$^+$ T cell memory responses at the mucosal tissue following the clearance of primary infection. To this end, we utilized a mouse model of influenza A virus PR8/34 (PR8) infection, in which viral clearance occurs within 10 days post infection (d.p.i.) [41, 42, 43]. We infected WT mice with PR8 virus and depleted CD4$^+$ T cells with α-CD4 (GK1.5, 250 μg/mouse/weekly) injection starting at 14 d.p.i. (Fig. 1a). CD4$^+$ T cells were largely depleted in the spleen and the lung as confirmed by flow cytometry (Extended Fig. 1a). At 42 d.p.i., we analyzed lung tissue B and T cell responses through intravenous (i.v.) injection of α-CD45 5 min before mouse sacrifice as we and others reported [40, 44, 45]. In this setting, $CD45_{i.v.}^-$ cells were within lung tissue, while $CD45_{i.v.}^+$ cells were in lung blood vessels. CD4$^+$ T cell depletion disrupted the formation of iBALT, which contained B cell and CD4$^+$ T cell aggregates [37, 46, 47] (Fig. 1b and Extended Fig. 1b). CD4$^+$ T cell depletion also abrogated lung B_{GC} responses (Extended Fig. 1c). We then examined influenza Hemagglutinin-specific B (HA-B) cell responses in the lungs and spleens following CD4$^+$ T cell depletion at 42 d.p.i. CD4$^+$ T cell depletion did not affect lung circulating ($CD45_{i.v.}^+$) nor splenic HA-specific B cell responses, but drastically diminished total and HA-specific B cells in the lung tissue at the memory stage (Fig. 1c and Extended Fig. 1d, e).

We next examined influenza-specific CD8$^+$ memory T cell responses in the lungs and spleens following CD4$^+$ T cell depletion. To do so, we checked lung CD8$^+$ memory T cell responses against two dominant influenza MHC-I H-2D^b-restricted epitopes, nucleoprotein peptide 366-374 ($NP_{366-374}$) and polymerase peptide 224-233 ($PA_{224-233}$) through tetramer staining at 42 d.p.i. [40]. It has been shown before that CD8$^+$ memory T cells against $NP_{366-374}$ or $PA_{224-233}$ epitope exhibit distinct phenotypic and recall properties [40, 48, 49, 50]. Specifically, lung CD8$^+$ $NP_{366-374}$ memory T cells are highly protective and dominate over the CD8$^+$ $PA_{224-233}$ memory T cells in the secondary recall expansion upon re-challenge with heterotypic influenza virus [40, 48, 49, 50]. We found that late CD4$^+$ T cell depletion did not affect lung circulating or tissue CD8$^+$ $PA_{224-233}$ memory T cell population (Fig. 1d and Extended Fig. 1f, g). However, late CD4$^+$ T cell depletion caused significant decrease of the magnitude of CD8$^+$ $NP_{366-374}$ memory T cells in the lung tissue

compartment but not in the circulation (Fig. 1d and Extended Fig. 1f, g). The magnitudes of parenchymal $CD8^+$ $CD69^+$ $NP_{366-374}$ T_{RM} or $CD8^+$ $CD69^+$ $CD103^+$ $NP_{366-374}$ T_{RM} cells were also diminished following late $CD4^+$ T cell depletion (Fig. 1d and Extended Fig. 1h). Notably, late $CD4^+$ T cell depletion did not affect the percentages of $CD103^+$ cells within the $CD8^+$ $CD69^+$ $NP_{366-374}$ T_{RM} population (Extended Fig. 1i), which is in contrast with the results observed following $CD4^+$ T cell depletion before influenza infection [30]. Contrary to the diminished magnitude of lung $CD8^+$ $NP_{366-374}$ T_{RM} cells, late $CD4^+$ T cell depletion did not decrease $CD8^+$ $NP_{366-374}$ or $CD8^+$ $PA_{224-233}$ memory T cells (T_{MEM}) in the lung vasculature or spleen (Fig. 1e and Extended Fig. 1g). Thus, these data suggest that continuous $CD4^+$ T cell help following viral clearance is required for the persistence of optimal B and $CD8^+$ T cell responses (against a dominant protective epitope) in the lung at the memory stage.

It is possible that $CD4^+$ T cells may provide the "help" either in the circulation or in the lungs for the generation of optimal tissue memory B and $CD8^+$ T cells. To determine whether lung tissue $CD4^+$ T cells can provide the "local help" for lung memory B and $CD8^+$ T cell generation, we infected WT mice with PR8 virus and depleted $CD4^+$ T cells at 14 d.p.i. in the presence of FTY720 (Fig. 1f), a chemical that blocks lymphocyte migration [51]. We confirmed that FTY720 treatment drastically diminished T and B cell circulation in the blood (Extended Fig. 2a). The depletion of $CD4^+$ T cells abolished B_{GC} cell development, total HA-specific B cells (HA-B) and strikingly HA-specific B_{RM} (HA-B_{RM}) cells (identified as $CD45_{i.v.}^-$ $B220^+$ $GL7^-$ IgD^- IgM^- $CD38^+$ HA^+, Extended Fig. 1j) in the lungs (Fig. 1 g-i) even in the presence of FTY720. $CD4^+$ T cell depletion also diminished lung tissue $CD8^+$ $NP_{366-374}$-specific T_{MEM}, $CD8^+$ $CD69^+$ T_{RM} and $CD8^+$ $CD69^+$ $CD103^+$ T_{RM} cells (Fig. 1j). Similar data were observed following $CD4^+$ T cell depletion in the presence of FTY720 during H3N2 X31 influenza virus infection (Extended Fig. 2 b-e). Thus, lung $CD4^+$ T cells can provide *in situ* "help" to local B and $CD8^+$ T cells for the optimal development of B_{GC}, B_{RM} and $CD8^+$ T_{RM} cells following viral clearance.

We next sought to examine whether lung tissue $CD4^+$ T cells are sufficient for the generation of B_{GC}, B_{RM} and $CD8^+$ T_{RM} responses following the clearance of the primary infection, in the absence of circulating $CD4^+$ T cells. To do so, we injected low or high doses of α-CD4 into PR8-infected WT mice at 14 d.p.i. Low dose α-CD4 treatment largely ablated $CD4^+$ T cells in

the circulating blood, but not in the lung parenchyma, while high dose α-CD4 injection depleted both circulating and lung parenchymal $CD4^+$ T cells (Extended Fig. 2 f-h). Strikingly, the high dose, but not the low dose, of α-CD4 treatment diminished the magnitude of lung B_{GC}, influenza NP (nucleoprotein)-specific B_{RM} and $CD8^+$ $NP_{366-374}$ T_{RM} (including $CD69^+$ T_{RM} or $CD69^+CD103^+$ T_{RM}) cells (Fig. 1 k-n). Taken together, our data suggest that lung tissue $CD4^+$ T cells, rather than $CD4^+$ T cells in the circulation, provide late "local help" for the optimal generation of B_{GC}, B_{RM} and $CD8^+$ T_{RM} responses following influenza infection.

Identification of a population of T_{FH}-like cells in the lung

We next sought to identify the lung $CD4^+$ T cell populations that may mediate the local help to B and/or $CD8^+$ T cells. To do so, we performed single cell (sc) RNA-seq on $CD45_{i.v.}^-$ lung parenchymal $CD4^+$ T cells at 28 d.p.i. Hierarchical clustering analysis identified 5 separated $CD4^+$ T cell populations within the lung parenchyma (Fig. 2a and Extended Fig. 3 a, b). These cell populations included Th1 effector/memory-like cells (expressing high levels of *Cxcr6/Tbx21* (T-bet), cluster 0), T cells recently entering the lungs or circulating effector memory T cells (expressing high *Klf2/S1pr1*, cluster 1), regulatory T cells (Treg, expressing *Foxp3*, cluster 2), Th17-like (expressing *Il17/Ccr6/Rora*, cluster 4) and a cluster of T cells exhibiting features of T_{FH} cells (expressing *Bcl6/Il21*, cluster 3) (Fig. 2b and Extended Fig. 3 a-c). Cluster 3 $CD4^+$ T cells also expressed higher levels of T_{FH}–associated surface molecules *Pdcd1*(PD-1), *Cxcr5* and *Izumo1r* (FR4) (Fig. 2b).

Flow cytometry analysis identified a population of total $CD4^+$ or influenza-specific $CD4^+$ $NP_{311-325}$ $PD\text{-}1^{Hi}FR4^{Hi}$ T cells that developed following influenza infection and expressed T_{FH}-associated markers including BCL6, ICOS and P2RX7, but relatively lower levels of CXCR5 compared to splenic T_{FH} cells (Fig. 2 c, d). Similar to splenic T_{FH} cells, lung $CD4^+$ $PD\text{-}1^{Hi}FR4^{Hi}$ T cells expressed low levels of IFN-γ and IL-17 (Fig. 2e). However, splenic T_{FH} cells expressed significantly higher IL-4 than lung $CD4^+$ $PD\text{-}1^{Hi}FR4^{Hi}$ T cells (Fig. 2 e). We next examined whether lung $CD4^+$ $PD\text{-}1^{Hi}FR4^{Hi}$ T cells expressed the T_{FH} signature cytokine IL-21 following influenza virus infection using the IL-21-VFP reporter mice [52]. Lung $CD4^+$ $PD\text{-}1^{Low}$ $FR4^{Low}$ T cell population expressed modest levels of IL-21, but the lung $CD4^+$ $PD\text{-}1^{Hi}FR4^{Hi}$ T cells expressed high levels of IL-21, almost comparable to those of splenic T_{FH} cells (Fig. 2f). These

data suggest that there is a lung tissue $CD4^+$ T cell population, transcriptionally and phenotypically resembling T_{FH} cells in the secondary lymphoid organs.

Transcriptional profiling reveals lung T_{FH}-like cells exhibit T_{RM} gene signature

To gain more insights into the phenotype and identity of lung T_{FH}-like cells, we sought to compare the transcriptional signatures of lung T_{FH}-like cells to splenic T_{FH}, non-T_{FH} and lung non-T_{FH}-like cell signatures. $Foxp3^+$ Treg cells expressed FR4, GITR and PD-1 (albeit their PD-1 levels were lower than T_{FH}-like cells) (Fig. 2b and Extended Fig. 3c and 4a). To minimize the potential contribution of Treg cells on the transcriptional profiles of lung T_{FH}-like cells, we excluded splenic or lung $GITR^+$ $CD4^+$ T cells, which were mostly $Foxp3^+$ cells, in our sorting (Extended Fig. 4a). We then sorted splenic non-T_{FH} ($CD4^+CD44^{Hi}GITR^-CXCR5^{Low}PD\text{-}1^{Low}$), splenic T_{FH} ($CD4^+CD44^{Hi}GITR^-CXCR5^{Hi}PD\text{-}1^{Hi}$), lung non-$T_{FH}$-like cells ($CD45_{i.v.}^-$ $CD4^+CD44^{Hi}GITR^-PD\text{-}1^{Low}FR4^{Low}$) and lung T_{FH}-like cells ($CD45_{i.v.}^-$ $CD4^+CD44^{Hi}GITR^-$ $PD\text{-}1^{Hi}$ $FR4^{Hi}$) cells and performed RNA-seq analysis.

Differential gene expression and principal component analysis revealed that those four different $CD4^+$ T cell populations have distinct gene expression patterns, although lung $CD4^+$ $PD\text{-}1^{Hi}FR4^{Hi}$ cells were more distinct from splenic non-T_{FH} cells relative to splenic T_{FH} or lung $CD4^+$ $PD\text{-}1^{Low}FR4^{Low}$ cells (Fig. 3a, b and Extended Fig. 4b). When directly compared to lung $CD4^+$ $PD\text{-}1^{Low}FR4^{Low}$ cells, lung $CD4^+$ $PD\text{-}1^{Hi}FR4^{Hi}$ cells highly expressed T_{FH}-associated genes including *Il21*, *Tox2* and *Pdcd1* (Fig. 3c). Indeed, Gene Set Enrichment Analysis (GSEA) showed that lung $CD4^+$ $PD\text{-}1^{Hi}FR4^{Hi}$ cells had enrichment of T_{FH}-associated genes [53] relative to $CD4^+$ $PD\text{-}1^{Low}FR4^{Low}$ cells (Fig. 3d). Conversely, lung $CD4^+$ $PD\text{-}1^{Low}FR4^{Low}$ cells expressed higher levels of *Ly6c* and *Il7r*, and showed enhanced enrichment of genes in TGF-β, hypoxia and Notch signaling relative to $PD\text{-}1^{Hi}FR4^{Hi}$ cells (Fig. 3c and Extended Fig. 4c). When compared to splenic T_{FH} cells, lung $CD4^+$ $PD\text{-}1^{Hi}FR4^{Hi}$ cells showed increased expression of genes associated with tissue migration, retention and function including *Ccr2, Bhlhe40* and *Cxcr6* (Fig. 3e) [54, 55]. GSEA analysis revealed that lung $CD4^+$ $PD\text{-}1^{Hi}FR4^{Hi}$ had significant enrichment of T_{RM}-associated genes relative to splenic T_{FH} cells (Fig. 3f) [56]. Lung $CD4^+$ $PD\text{-}1^{Hi}FR4^{Hi}$cells also had higher expression of genes associated with IL-2/STAT5, NF-κB and interferon signaling, whereas splenic T_{FH} cells had higher enrichment of Myc and PI3K-mTOR signaling (Extended

Fig. 4d). Thus, these RNA-seq analyses indicate that lung CD4$^+$ PD-1^{Hi}FR4^{Hi} cells exhibit transcriptional signatures of both T_{FH} cells and T_{RM} cells.

To confirm these observations, we sorted splenic T_{FH}, lung CD4$^+$ PD-1^{Hi}FR4^{Hi} or lung CD4$^+$ PD-1^{Low}FR4^{Low} cells and performed Nanostring analysis of 560-immune associated genes without the need of RNA amplification [40]. Compared to lung CD4$^+$ PD-1^{Low}FR4^{Low} cells, splenic T_{FH} and lung CD4$^+$ PD-1^{Hi}FR4^{Hi} cells expressed higher levels of T_{FH}-associated genes including *Bcl6, Sh2d1a* and *Tcf7* (Fig. 3g). Compared to splenic T_{FH} cells, both PD-1^{Hi} FR4^{Hi} and PD-1^{Low} FR4^{Low} lung CD4$^+$ T cell populations had enhanced expression of genes associated with tissue migration and residency, but diminished expression of lymphoid migration or retention molecules *Sell* (CD62L) and *Ccr7* (Fig. 3h). Altogether, these data suggest that lung CD4$^+$ PD-1^{Hi}FR4^{Hi} cells exhibit a "hybrid" gene signature of both conventional T_{FH} cells and T_{RM} cells.

Lung CD4$^+$ PD-1^{Hi} FR4^{Hi} T cells are tissue-resident

Given that lung CD4$^+$ PD-1^{Hi}FR4^{Hi} cells showed gene signatures of tissue residency, we sought to determine whether these cells are indeed tissue-resident. Using flow cytometry, we confirmed that PD-1^{Hi}FR4^{Hi} cells expressed higher levels of CD69, CXCR6 and *Bhlhe40*, molecules associated with T cell migration, retention and function in the respiratory mucosal tissue, compared to splenic T_{FH} cells (Fig. 4a). We then performed parabiosis experiments and joined the circulation of PR8-infected CD45.1$^+$ and CD45.1$^+$ CD45.2$^+$ congenic mice at 21 d.p.i. (Fig. 4b). We examined CD4$^+$ T cell exchange between the two parabionts after 2 weeks of parabiosis. Close to 40-60 % of splenic CD4$^+$ T cells in parabiont hosts were derived from their parabiont pair (Fig. 4c), suggesting the successful exchange of circulating CD4$^+$ T cells between the parabionts. Within lung i.v. CD45 antibody (Ab) protected tissue CD4$^+$ T cell compartment, PD-1^{Hi}FR4^{Hi} total CD4$^+$ or antigen (Ag)-specific CD4$^+$ $NP_{311-325}$ T cells exhibited limited exchange between the two parabionts (Fig. 4d, e), suggesting that these cells are mostly tissue-resident. Of note, most of Ag-specific CD4$^+$ $NP_{311-325}$ T cells are tissue-resident (Fig. 4e), while total lung CD4$^+$ PD-1^{Low}FR4^{Low} T cells showed higher circulating rate than those of CD4$^+$ PD-1^{Hi}FR4^{Hi} cells (Fig. 4 d). Thus, lung CD4$^+$ PD-1^{Hi}FR4^{Hi} cells are lung tissue-resident T cells exhibiting both T_{FH} and T_{RM} features. Based on their gene signature, protein expression, cytokine production and tissue residency property, we termed these cells as tissue-resident T helper (T_{RH})

cells.

T_{RH} responses require B cells and lung tertiary lymphoid structure formation

T_{FH} generation requires the presence of B cells [57]. We therefore examined whether lung B cells are required for the generation of T_{RH} cells following influenza infection. To do so, we infected WT mice with PR8 and then depleted B cells with α-CD20 treatment in the presence of FTY-720 to block T/B cell migration (Fig. 5a). We validated that α-CD20 treatment depleted lung B cells (Extended Fig. 5a). We then determined splenic T_{FH} and lung T_{RH} responses with or without α-CD20 treatment at 28 d.p.i. Consistent with previous findings [58], B cell depletion following α-CD20 treatment diminished splenic T_{FH} responses (Fig. 5b). α-CD20 treatment also impaired lung T_{RH} responses, but not lung non-T_{RH} (PD-1^{Low}FR4^{Low}) responses. Thus, lung B cells are required for the development of T_{RH} responses. Tertiary lymphoid structures (iBALT) form in the lung that consist of aggregated B, T and dendritic cells (DCs) following influenza viral clearance [37, 46, 47]. IL-21 expressing lung $CD4^+$ T cells were found in the iBALT from PR8-infected IL-21-VFP reporter mice (Extended Fig. 5b), suggesting that iBALT formation may be required for optimal T_{RH} responses following influenza virus clearance. To this end, we infected WT mice with PR8 and then injected the mice with lymphotoxin beta receptor Ig fusion protein (LTβR-Ig) in the presence of FTY-720 to deplete iBALTs in the lungs [59, 60] (Fig. 5a). We confirmed that LTβR-Ig injection diminished lung iBALT formation and the magnitude of lung parenchyma B cell expansion (Fig. 5c and Extended Fig. 5c). LTβR-Ig injection did not affect splenic T_{FH} responses, but significantly impaired influenza-specific lung T_{RH} but not non-T_{RH} responses (Fig. 5d). Thus, these data indicate that lung tissue B cells and iBALT formation is required for the optimal generation of lung T_{RH} responses.

Optimal T_{RH} responses depend on both T_{FH} and T_{RM} transcription factors

We next sought to investigate the molecular mechanisms regulating lung T_{RH} cell development following influenza virus infection. We first examined whether lung T_{RH} cell development is dependent on the master transcription factor of T_{FH} cells, BCL6 [61, 62]. To do so, we infected WT (*Bcl6*$^{fl/fl}$) or *Bcl6*$^{\Delta T}$ mice with PR8 virus and examined total and influenza-specific T_{RH} or non-T_{RH} cells in the lung tissue at 28 d.p.i. We found that T cell-specific BCL6 deficiency greatly diminished both the frequencies and the magnitude of lung T_{RH} responses, but not those of non-

T_{RH} responses (Fig. 6a-c). Consistent with the literatures [57, 63], T cell-specific BCL6 deficiency also diminished splenic T_{FH} responses (Fig. 6d, e).

We have demonstrated before that Bhlhe40 is critical for the development of tissue-resident $CD8^+$ T cell responses [55]. Since lung T_{RH} and non-T_{RH} cells expressed high levels of *Bhlhe40* relative to splenic T_{FH} cells (Fig 4a), we investigated the roles of Bhlhe40 in lung T_{RH} responses relative to splenic T_{FH} cells. Consistent with high Bhlhe40 expression in T_{RH} cells, lung T_{RH} cells were enriched with Bhlhe40-associated genes [55] compared to splenic T_{FH} cells (Fig. 6f). We then infected WT (*Bhlhe40*$^{fl/fl}$) or *Bhlhe40*$^{\Delta T}$ mice with PR8 and examined total and influenza-specific T_{RH} or non-T_{RH} cells at 28 d.p.i. T cell-specific Bhlhe40 deficiency modestly increased the frequencies of T_{RH} cells relative to non-T_{RH} cells within the influenza-specific $NP_{311-325}$ $CD4^+$ T cell population, but not in the total lung $CD4^+$ T cell population (Fig. 6g, h and Extended Fig. 5 e). Bhlhe40-deficiency in T cells significantly diminished total and influenza-specific $CD4^+$ T cells in the lung tissue, but not in the spleen (Extended Fig. 5 f, g). These data suggest that Bhlhe40 is required for the establishment of the overall lung-resident $CD4^+$ T cell population following influenza infection, as was observed with the lung-resident $CD8^+$ T cells [55]. As the result, the magnitude of both T_{RH} and non-T_{RH} cells in the lungs were significantly decreased (Fig. 6i). In contrast, Bhlhe40 deficiency did not alter either the frequencies or the magnitude of the splenic T_{FH} response (Fig. 6g-i and Extended 5 d, e). Previously, we have reported that Bhlhe40 is required for the survival $CD8^+$ T cells in non-lymphoid tissues [55]. Consistent with that observation, Bhlhe40 deficiency resulted in enhanced cellular apoptosis in both lung T_{RH} and non-T_{RH} cells (Fig. 6j, k). These data indicate that Bhlhe40 is likely not important for the acquisition of "T_{FH}-like" features in T_{RH} cells, but is vital in sustaining T_{RH} cell survival in the respiratory mucosal tissues. Taken together, the optimal formation of lung T_{RH} cells requires transcription factors involved in both T_{FH} (BCL6) and T_{RM} (Bhlhe40) development. Conversely, the formation of splenic T_{FH} cells is dependent on BCL6 but not Bhlhe40, and the development of lung PD-1^{Low}FR4^{Low} cells (probably consist of conventional T_{RM} cells) is dependent on Bhlhe40 but not BCL6.

T_{RH} cells assist the formation of protective B_{GC}, B_{RM} and $CD8^+$ T_{RM} responses

We hypothesize that T_{RH} cells are those cells mediating the effects of $CD4^+$ T cell help on lung

local B and $CD8^+$ T cells. Consistent with that hypothesis, T cell-specific BCL6 deficiency leaded to diminished iBALT formation, B_{GC}, B_{RM} and $CD8^+$ $NP_{366-374}$ T_{RM} responses (Extended Fig. 6 a-d). Furthermore, T cell-specific Bhlhe40 deficiency also resulted in diminished lung tissue B cells, B_{RM} and $CD8^+$ T_{RM} responses, although it is possible that Bhlhe40 deficiency in $CD8^+$ T cells directly contribute to the diminished $CD8^+$ T_{RM} phenotype in these mice as shown before [55] (Extended Fig. 6 e-g).

To specifically determine whether T_{RH} cells are required for the development of memory B and $CD8^+$ T cells in the lungs, we generated CD4 T cell -specific inducible BCL6-deficient mice (*Bcl6*$^{\Delta CD4\ ERT2}$). We first confirmed that tamoxifen treatment efficiently caused gene recombination in $CD4^+$ T cells, but only minimally in other lymphocytes in *Bcl6*$^{\Delta CD4\ ERT2}$ mice (Extended Fig. 7a-c). We then infected WT (*Bcl6*$^{fl/fl}$) or *Bcl6*$^{\Delta CD4\ ERT2}$ mice with PR8 and inoculated tamoxifen daily from 12 to 16 d.p.i. (5X) to specifically ablate BCL6 in $CD4^+$ T cells following influenza infection (Fig. 7a). To exclude the contribution of lymphoid organ T_{FH} cells in providing the "late" help to lung B and $CD8^+$ T cells, we treated the mice with FTY720 daily to block T and B cell migration starting at 11 d.p.i. At the lung, the magnitude of $CD45_{i.v.}^-$ $CD4^+$, $CD8^+$ T and B cells was decreased in inducible BCL6 ablated group (Extended Fig. 7d). As with the constitutive BCL6 deficiency in T cells, inducible $CD4^+$ T cell-specific BCL6 ablation resulted in diminished T_{RH} but not non-T_{RH} responses in the lungs (Extended Fig. 7e). Strikingly, the ablation of lung T_{RH} responses significantly diminished B_{GC}, influenza HA-specific B_{RM} (HA-B_{RM}) and NP-specific B_{RM} (NP-B_{RM}) responses in the lungs (Fig. 7b-d). $CD8^+$ $NP_{366-374}$ T_{RM} responses were also significantly impaired following T_{RH} ablation (Fig. 7e). Together these data suggest that lung T_{RH} cells are important in assisting the development of local B and $CD8^+$ memory responses *in situ* in the respiratory tract.

To examine the roles of T_{RH} cells in the maintenance of lung tissue B and $CD8^+$ T cell responses, we treated WT or *Bcl6*$^{\Delta CD4\ ERT2}$ mice with tamoxifen starting from 21 to 25 d.p.i. to ablate T_{RH} cell responses at the memory stage (Fig. 7f). We then examined B_{GC}, B_{RM} and $CD8^+$ T_{RM} responses at 42 d.p.i. (Fig. 7g-j). T_{RH} ablation at the memory stage did not lead to significant decrease of B_{RM} magnitude, but significantly impaired B_{GC} responses at 6 weeks post infection (Fig. 7g-i). These data suggest T_{RH} cells help to program lung B_{RM} cell development, but may

not be directly required for their maintenance at the memory stage. However, T_{RH} cells are continuously needed for sustaining lung B_{GC} responses (Fig. 7g). Notably, these data are consistent with the data showing that B_{GC} responses are important for B_{RM} cell development in the first three weeks, but may not significantly contribute to lung B_{RM} cells after 20 d.p.i. [5]. T_{RH} ablation at the memory stage also diminished $CD8^+$ $NP_{366-374}$ T_{RM} responses, suggesting that lung T_{RH} cells continuously provide "local help" for the maintenance of $CD8^+$ $NP_{366-374}$ T_{RM} cells (Fig. 7j). Taken together, our data suggest that T_{RH} cells are vital for programming lung B_{RM} cell development before 20 d.p.i., but are necessary for both the optimal development and maintenance of B_{GC} and $CD8^+$ $NP_{366-374}$ T_{RM} responses at the memory stage.

Previously, it was shown that lung memory B cells generated from local B_{GC} cells harbored high portions of cross-reactive B cells following influenza X31 virus infection (H3N2 virus) [14]. To examine whether T_{RH} cells help to generate those cross-reactive B_{RM} cells, we infected WT or *Bcl6*$^{\Delta CD4ERT2}$ mice with X31 virus and injected the mice with tamoxifen in the presence of FTY720 as in Extended Fig. 7a. We then checked X31 strain-specific HA-B_{RM} and cross-reactive HA-B_{RM} against H3N2 A/Uruguay/716/07 strain (Urg) [14] using flow cytometry. T_{RH} ablation resulted in diminished strain-specific (X31 HA^+ and Urg HA^-) and cross-reactive (both X31 HA^+ and Urg HA^+) B_{RM} responses (Fig. 7k), indicating potential roles of T_{RH} cells in the development of both strain-specific and cross-reactive B cell immunity.

Since $CD8^+$ T_{RM} (particularly $NP_{366-374}$ T_{RM} [40]) and possibly B_{RM} cells are important in mediating host heterologous protection [5], we next sought to determine whether the ablation of T_{RH} cells impairs host protective immunity against heterologous virus infection. To do so, we employed a heterologous infection and challenge model in which X31 virus was used as the primary infection and lethal PR8 virus was used as secondary challenge [55]. PR8 and X31 viruses differ in the viral surface proteins but share internal viral proteins such as NP [64]. As such, $CD8^+$ T_{RM} and possibly B_{RM} cells against internal viral epitopes (mainly against viral NP protein) can provide heterologous protection [5, 40]. We infected WT or *Bcl6*$^{\Delta CD4ERT2}$ mice with X31 virus and treated the mice with tamoxifen. We confirmed that T_{RH} ablation affects CD8 $NP_{366-374}$ T_{RM}, B_{GC} and B_{RM} development in the X31 model at 35 d.p.i. (Extended Fig. 7f). We then re-challenged the mice with a lethal dose of PR8 in the presence of FTY720 to block the contribution of circulating

memory $CD8^+$ T and B cells at 42 d.p.i. (Fig. 7l). Close to 40% of *Bcl6*$^{\Delta CD4ERT2}$ mice succumbed, while WT mice were fully protected with lethal PR8 infection (Fig. 7m). Thus, we conclude that T_{RH} cells are required for the optimal protection against secondary heterologous infection, most likely through their help for the development of protective CD8 T_{RM} and B_{RM} response.

Identification of the factors mediating T_{RH}-derived "local" help.

We next sought to identify the underlying mechanisms by which T_{RH} cells promote B cell and $CD8^+$ T_{RM} immunity. As shown in Fig. 2, T_{RH} cells expressed high levels of *Il21*. To identify the major IL-21-expressing cell types in the lung, IL-21-VFP reporter mice were infected with PR8 and examined at 28 d.p.i. The vast majority of lung IL-21-VFP^+ cells were $CD4^+$ T cells (Fig. 8a). IL-21-VFP^{hi} cells, which expressed the highest levels of IL-21 than those IL-21-VFP^{low} cells (Extended Fig. 8a), were mainly T_{RH} cells (Fig. 8b). Additionally, T cell-specific BCL6 deficiency impaired *Il21* expression in the lungs (Extended Fig. 8b). These data suggest that T_{RH} cells are the main IL-21 producers in the lungs following influenza virus infection.

Since IL-21 is an important cytokine that has been implicated in facilitating B_{GC}, memory B and $CD8^+$ effector and memory T cell responses [65], we blocked IL-21 signaling starting at 14 d.p.i. through intraperitoneal injection of α-IL-21R in the presence of FTY720 (Fig. 8c). To our surprise, IL-21 signaling blockade did not impair B_{GC} or influenza HA-specific B_{RM} responses in the lung tissue (Fig. 8d, e). However, IL-21 signaling blockade significantly diminished $CD8^+$ $NP_{366-374}$ T_{RM} responses, suggesting that T_{RH} cells help $CD8^+$ T_{RM} establishment and/or maintenance through IL-21 (Fig. 8f). We also blocked IL-21 signaling locally in the lung through intranasal delivery of α-IL-21R (Fig. 8g). Lung local blockade of IL-21 signaling diminished lung $CD8^+$ $NP_{366-374}$ T_{RM} magnitude, but not splenic memory T cells (Fig. 8h, i). Local blockade of IL-21 signaling also did not affect B_{GC} or HA-specific B cell responses in the lung parenchymal compartment (Extended Fig. 8c).

Consistent with the diminished $CD8^+$ $NP_{366-374}$ T_{RM} responses, IL-21R signaling blockade leaded to enhanced cellular apoptosis but not proliferation, specifically in $CD8^+$ $NP_{366-374}$ T_{RM} but not those of splenic memory T cells (Fig. 8j, k). Of note, compared to $CD8^+$ $PA_{224-233}$ T_{RM} cells, $CD8^+$ $NP_{366-374}$ T_{RM} cells exhibited higher expression of genes associated with IL-21 signaling

including *Batf* (Extended Fig. 8d, e) [66]. These data suggest that $CD8^+$ $NP_{366-374}$ T_{RM} cells, but not $CD8^+$ $PA_{224-233}$ T_{RM} cells, potentially receive IL-21 signaling in the lungs at the memory stage following influenza virus infection. Consistent with the data, we found that IL-21R blockade diminished BATF expression in $CD8^+$ $NP_{366-374}$ T_{RM}, but not $CD8^+$ $PA_{224-233}$ T_{RM} cells at 35 d.p.i. (Fig. 8l). Taken together, these data suggest T_{RH} cells provide local help for the development of $CD8^+$ $NP_{366-374}$ T_{RM} cells in an IL-21-dependent manner.

CD40-CD40L interaction is critical for T cell help of B_{GC} cell responses [5, 57]. Previously, it was shown that lung B_{GC} cells contributed to lung local B_{RM} cell responses [14]. Furthermore, diminished B_{GC} response following CD40L blockade can lead to impaired B_{RM} formation when α-CD40L was given before 20 d.p.i., although it is unknown whether this is due to diminished lung or circulating B_{GC} responses [5]. Lung influenza-specific T_{RH} cells express higher levels of CD40L than non-T_{RH} cells (Fig. 8m and Extended Fig. 8f). To determine whether CD40L promotes lung B_{GC} responses to facilitate local B_{RM} formation following influenza infection, we inoculated α-CD40L into PR8-infected mice at 14 d.p.i. in the presence of FTY720 as of Fig. 8c. As shown in Fig. 8n and o, CD40L blockade greatly diminished lung B_{GC} formation and the magnitude of HA-specific B_{RM} responses in the lung tissue. These data indicate that T_{RH} cells facilitate B_{GC} and B_{RM} responses through CD40L-dependent mechanisms.

Discussion

In this report, we have discovered a previously unrecognized requirement for "*in situ*" CD4$^+$ T cell help in the respiratory mucosa, which is mediated by what we have termed T_{RH} cells, in the development of localized protective memory responses following influenza virus infection. T_{RH} cells co-manifest phenotypic and transcriptional hallmarks of both T_{FH} and T_{RM} cells. We have further identified the cellular and molecular mechanisms guiding the development of T_{RH} cells, and key factors mediating their helper function to B and CD8$^+$ T cells (Extended Fig. 8g).

The expression of T_{FH}-associated molecules by T_{RH} cells appear to be lower compared to those of splenic T_{FH} cells (such as BCL6 and CXCR5). These PD-1^{Hi} CXCR5^{Low} BCL6^{Int} T_{FH}-like cells have been previously observed [34, 35, 36, 37, 38]. However, the cellular identity and developmental cues regulating their development remain largely elusive. Furthermore, the physiological function of these cells beyond their help on the generation of B_{GC} cells are currently unknown. Using total and single cell transcriptional profiling and phenotypic analysis combined with parabiosis, we have identified that these tissue T_{FH}-like cells exhibit enhanced expression of molecules-associated with peripheral migration and tissue residency, and show limited circulating ability. We therefore term these cells as T_{RH} cells based on their transcriptional signature, non-migratory features and helper function. Currently, the cellular origins of these T_{RH} cells are not determined in this study. T cell priming occur in the draining lymph nodes and it is possible that T_{RH} cells originate from those lymph node pre-T_{FH} or interfollicular T_{FH} cells (T_{FH} precursors outside the GC [67, 68]) entering circulation and adopting T_{RM} signatures following entry in the lung parenchymal environment. Conversely, it is also possible that T_{RH} cells develop from Th1-polarized cells and adopt "T_{FH}-like" features in the iBALT structure when interacting with B cells. These possibilities of T_{RH} cell development warrant further investigation. Nevertheless, based on the T_{RH} transcriptional profiles and the dual requirement of BCL6 and Bhleh40 for their formation, we believe that T_{RH} cells are likely a "hybrid" of T_{FH} and T_{RM} cells, and may represent a unique population present in various tertiary lymphoid structures of mucosal tissues.

Lung T_{RH} cells appear to be required for programing localized memory B and T cell responses in the respiratory mucosal tissue. Previously, it was shown that locally-generated lung B_{GC} cells

contribute significantly to the lung B_{RM} cell pool following influenza virus infection [14]. Thus, T_{RH} cells assist the development of B_{RM} responses likely due to their help for the generation of lung B_{GC} cells, rather than their direct "help" on lung B_{RM} cells per se for their differentiation and/or maintenance. Consistent with this idea, the ablation of T_{RH} cells around 4 weeks post infection did not significantly impact lung B_{RM} cell maintenance. In accordance, the inoculation of CD40L Ab after 3 weeks of infection, which blocked the generation of lung B_{GC} cells, fails to impact B_{RM} cell generation [5]. These data suggest that localized B_{GC} responses in the iBALT, programmed by lung T_{RH} cells in the first three weeks of infection, facilitate B_{RM} development following influenza virus infection.

Beyond their help to B cells, T_{RH} cells are required for the optimal responses of a protective $CD8^+$ T_{RM} population, most likely through the production of IL-21. Of note, it was previously shown that continuous $CD4^+$ T cell help beyond T cell priming was not required for the differentiation of $CD103^+$ $CD8^+$ T_{RM} cells [30]. Consistently, we found that $CD4^+$ T cell depletion following the resolution of primary infection did not impact CD103 expression by $CD8^+$ T_{RM} cells. However, persistent "late" help following viral clearance is required for the generation and/or the maintenance of a protective lung T_{RM} population in our study. The timing of $CD4^+$ T cell depletion (day 7 previously [30] versus day 14 $CD4^+$ T cell depletion used here) likely explains the differences observed in the two models. It is possible that early depletion of $CD4^+$ T cells before viral clearance (i.e. day 7) alters lung viral and/or inflammatory environment, which compensate the requirement of lung $CD4^+$ T cells for $CD8^+$ T_{RM} programming and/or maintenance. Other possibilities, including infection schemes and the levels of $CD4^+$ T cell depletion following α-CD4 inoculation may also contribute to the differences observed. Nevertheless, using multiple lines of approaches including high or low doses of α-CD4 depletion, inducible $CD4^+$ T cell-specific BCL6 ablation and IL-21 blockade combined with long-term FTY720 treatment, we have provided comprehensive evidence that localized $CD4^+$ T cell help, mediated by T_{RH} cells and IL-21, is required for the optimal generation of a population of protective T_{RM} cells ($H2D^b$-restricted $NP_{366-374}$ T_{RM} cells) following the resolution of primary infection.

Then, the question is why lung T_{RH} help, in the form of IL-21 provision, is specifically required for $CD8^+$ $NP_{366-374}$ T_{RM} responses. We have shown previously that $CD8^+$ $NP_{366-374}$ T_{RM} cells receive constant antigen engagement in the lungs at the memory stage due to the chronic deposition of high levels of influenza NP antigen [40]. Compared to conventional $CD8^+$ $PA_{224-233}$ T_{RM} cells, $CD8^+$ $NP_{366-374}$ T_{RM} cells express high levels of PD-1 and exhibit "exhausted-like" phenotypes similar to those of T cells receiving chronic antigen exposure during chronic viral infections [40, 69, 70]. Consequently, the maintenance of these T_{RM} cells requires persistent MHC I-dependent stimulation at the memory stage [40], similar to those of exhausted $CD8^+$ T cells [69]. Notably, $CD4^+$ T cell help in the form of IL-21 has been recently demonstrated to sustain those PD-1-expressing $CD8^+$ T cells during chronic viral infection and tumor growth [71]. Thus, $CD4^+$ T cell help and IL-21 signaling may be specifically required for maintaining the survival of lung $CD8^+$ T_{RM} cells receiving persistent low levels of *in situ* antigenic stimulation. Consistent with this idea, $NP_{366-374}$ T_{RM} cells express higher levels of molecules associated with IL-21 signaling, particularly BATF.

Influenza virus is able to undergo antigenic shift, drift and re-assortment to escape previously established host immunity. Current influenza vaccines require yearly update and only provide high levels of protection when influenza vaccine strains match exactly with the circulating strains. Much of attention has been given to the development of potential universal influenza vaccines recently. The common goals of various universal influenza vaccine candidates are to induce broadly neutralizing influenza Ab, strong $CD8^+$ memory T cell responses against conserved epitopes and/or high levels of localized lung-resident mucosal immunity that can restrict viral spreading early [72, 73, 74, 75]. Due to the high mutation rates of influenza viruses, it is conceivable that the induction of "all inclusive" immune responses, i.e. induction of strong both B and $CD8^+$ T cell immunity in the mucosal tissue, may be required for the ultimate success of a universal influenza vaccine [75]. Due to the unique ability of T_{RH} cells in assisting local B_{RM} and T_{RM} development, it is tempting to speculate that the specific promotion of T_{RH} cells may simultaneously promote both memory B and $CD8^+$ T cell immunity in the respiratory tract during vaccination, thereby providing rapid cross-reactive protection against broad-spectrum viruses.

Acute influenza virus infection can lead to the development of chronic lung pathogenic sequelae [40, 76]. The roles of iBALT and T_{RH} in the development of chronic lung conditions following influenza infection needs further investigations. Additionally, tertiary lymphoid (B/T) aggregates or iBALT-like structures have been observed in many chronic lung diseases including asthma, pulmonary fibrosis, COPD (Chronic obstructive pulmonary disease) etc [77, 78, 79, 80]. It was speculated that these tertiary lymphoid structures may play important roles in modulating the disease progression in those chronic lung conditions [47, 79]. T_{RH} cells may therefore participate in the regulation of chronic lung disease development. Further, recent advances have suggested that the development of tertiary lymphoid structures consisting of $CD4^+$ T and B cell clusters inside tumor effectively predicts patient responses to checkpoint blockade (anti-PD-1 and/or anti-CTLA4) therapies [81, 82, 83]. Given the transcriptional similarity of T_{RM} cells and tumor infiltrating lymphocytes (TILs) [84], it is possible that those T_{FH}-like cells present inside those tertiary lymphoid structures within tumor also exhibit tissue-resident signatures (i.e. T_{RH}-like cells). Indeed, a previous report has suggested the development of $CXCL13^+$ (human T_{FH} marker) $BHLHE40^+$ $CD4^+$ T cells are associated with enhanced responsibility to anti-PD therapy in colorectal cancer [85]. Thus, it is possible that T_{RH}-like cells may also provide "*in situ*" help for the optimal generation and/or maintenance of anti-tumor CD8 TILs following checkpoint blockade.

In summary, our data have revealed a complex T-B interaction network that is programed by lung T_{RH} cells for the maintenance of protective local respiratory immunity following acute influenza virus infection. Moving forward, it is of substantial interest to dissect the mechanisms modulating the development of T_{RH} cells and the precise function of T_{RH} cells in assisting the development of local B and CD8 T cell immunity during infection, vaccination and possibly cancer.

Materials and methods

Mice and influenza viral infection

WT C57BL/6, CD45.1 and IL-21 VFP reporter mice were purchased from the Jackson Laboratory (JAX) and bred in-house. To generate $CD45.1^+$ and $CD45.2^+$ ($CD45.1^+/CD45.2^+$) mice, CD45.1 mice were crossed with C57BL/6 mice. *Bcl6*$^{fl/fl}$ were generated as previously reported [63]. *Bcl6*$^{\Delta T}$ were generated by crossing with CD4-Cre transgenic. *Bcl6*$^{\Delta CD4ERT2}$ were generated by crossing with CD4-ERT2 transgenic mice. *Bcl6*$^{fl/fl}$ or *Bcl6*$^{\Delta CD4ERT2}$ mice were additionally crossed with Rosa26 LSL-YFP (JAX) mice for the determination of the efficiency of tamoxifen induced gene recombination. *Bhlhe40*$^{fl/fl}$ or *Bhlhe40*$^{\Delta T}$ mice were generated as previously reported [55]. All animal protocols were approved by the Institutional Animal Care and Use Committees (IACUC) of the Mayo Clinic (Rochester, MN). Sex-matched and age-matched 8- to 10-week-old mice of both sexes were used in the experiments. Influenza A/PR8/34 (~200 pfu/mouse in the primary infection and ~1×10^4 pfu/mouse in the secondary infection) and Influenza A X31 (~800 pfu/mouse in the primary infection) were infected into the mice by intranasal (i.n.) under anesthesia as reported before [42].

Intravascular labeling with α-CD45 and preparation of lung cell suspension

Mice were intravenously (i.v.) injected with 2 μg of α-CD45 (Clone: 30-F11) (Tonbo Biosciences) diluted in 300 μL of sterile PBS five minutes before sacrifice. To prepare single cells from lung tissue, lungs were cut into small pieces, digested with Type 2 Collagenase (Worthington Biochemical) and dissociated in 37°C for 30 min with Gentle-MACS (Miltenyi). Cells were further ground through 70μm cell strainer (Falcon) and washed with plain IMDM (Gibco). After red blood cell lysis, cells were centrifuged and re-suspended in cold FACS buffer (PBS, 2 mM EDTA, 2 % FBS, 0.09 % Sodium Azide) for flow cytometry analysis. Lung circulating immune cells are i.v. Ab^+ and lung tissue immune cells are defined by i.v. Ab^-. Lung T_{RM} cells were defined as $CD45_{i.v.}^-CD8^+$ $tetramer^+CD69^+$. Lung B_{RM} cells were defined as $CD45_{i.v.}^-$ $B220^+$ $GL7^-$ IgD^- IgM^- $CD38^+$ influenza B cell antigen (HA or NP)$^+$.

Antibody administration *in vivo*

Influenza infected WT mice were administrated with control IgG or various neutralizing or depleting Ab as described in the text. For CD4 T cell depletion with high dose of α-CD4, mice

were injected with 250 μg α-CD4 weekly (Clone: GK1.5, BioXCell) starting at 14 d.p.i. For circulating CD4 T cell depletion, mice were I.P. injected with 40 μg α-CD4 for the first dose followed with 10 μg α-CD4 weekly. For B cell depletion, mice were injected with 500 μg of α-CD20 (Clone: 5D2, Genentech). CD40L blockade or iBALT depletion were achieved by the injection of 250 μg of α-CD40L (Clone: MR-1, BioXCell) or 250 μg of LTβR-Ig weekly respectively. For systemic IL-21R blockade, 500 μg of α-IL21R (Clone: 4A9, BioXCell) was injected through I.P weekly starting at 14 d.p.i. For lung local IL-21R blockade, 50 μg of α-IL21R was injected through intranasal route (I.N.) weekly starting at 14 d.p.i. In some experiments, FTY720 (1 mg/kg) (Cayman) was administrated daily from 13 d.p.i. to block lymphocyte migration until mouse euthanasia.

Tamoxifen treatment

To induce gene recombination in *Bcl6*$^{\Delta CD4ERT2}$ mice, tamoxifen (Sigma-Aldrich) was diluted in warm sunflower oil (Sigma-Aldrich) and daily treated via intraperitoneal route for 5 consecutive times. Each application was 2 mg per mouse.

Flow cytometry analysis

For cell surface staining, cells were incubated with the appropriate antibody cocktail with FACS buffer for 30 min at 4 °C dark condition. Then cells were washed with FACS buffer. For intracellular staining, cell suspensions were stained with indicated surface markers and then washed with FACS buffer. Cells were then fixed and permeabilized with either Perm Fix and Wash buffer (Biolegend, for cytokine staining) or the Foxp3 transcription factor staining buffer set (eBioscience, for KI-67, Foxp3, BATF and BCL6 staining) for 1 hour at room temperature (RT) in the dark. Cells were washed twice with Perm Wash buffer (Biolegend or eBioscience) and stained with indicating Abs for 1 hour at RT. After staining, cells were washed again with Perm Wash buffer before flow cytometry acquisition. FACS Abs were primarily purchased from Biolegend, BD Biosciences, eBioscience or Tonbo Biosciences. The clone number of those Abs are as follows: CD45 (Clone: 30-F11), CD45.1 (Clone: A20), CD45.2 (Clone: 104), CD4 (Clone: RM4-5), CD44 (Clone: IM7), PD-1 (Clone: 29F.1A12), FR4 (Clone: eBio12A5), GITR (Clone: DTA-1), B220 (Clone: RA3-6B2), FAS (Clone: SA367H8), GL7 (Clone: GL7), CD38 (Clone: 90), IgD (Clone: 11-26c.2a), IgM (Clone: 11/41), CD8a (Clone: 53-6.7), CD69 (Clone: H1.2F3),

CD103 (Clone: 2E7), CXCR5 (Clone: SPRCL5), ICOS (Clone: 7E.17G9), P2RX7 (Clone: 1F11), CXCR6 (Clone: SA051D1), CD40L (Clone: MR1), BCL6 (Clone: K112-91), Foxp3 (Clone: 3G3), BATF (Clone: S39-1060), Ki67 (Clone: SoLA15), Streptavidin, IFN-γ (Clone: XMG1.2), IL-17 (Clone: TC11-18H10.1) and IL-4 (Clone: 11B11). The expression of Bhlhe40 was measured with Primeflow kit (Thermo Fisher Scientific). For CD40L staining, lung cells were pre-activated with 100 ng/mL of PMA and 1 μg/mL of ionomycin (Sigma-Aldrich) for 3 hrs in the 37°C before CD40L surface staining. H-2D^{b}-NP$_{366–374}$, H-2D^{b}-PA$_{224–233}$ and I-A^{b}-NP$_{311-325}$ tetramers were obtained from the National Institutes of Health tetramer facility. After Ab staining, cells were acquired with an Attune NxT system (Life Technologies). Data analysis was performed by FlowJo software (Tree Star).

B cell antigens

Influenza PR8-HA protein was a gift from Dr. Michelle C. Crank (NIH). PR8-NP protein was purchased from Sino Biological. Purified antigens were biotinylated using an EZ-Link Sulfo-NHS-LCBiotinylation kit (Thermo Fisher Scientific) using a 1:1.3 M ratio of biotin to Ag. To make tetramers, biotinylated Ags were mixed with streptavidin–PE (PJ27S; ProZyme) at the ratio determined or at a 5 to 1 ratio using the biotin concentration provided by the manufacturer as described before [86]. Following a 30-min incubation on ice, unconjugated biotinylated Ag was often removed by several rounds of dilution and concentration using a 100 kDa Amicon Ultra (MilliporeSigma) or 300 kDa Nanosep centrifugal devices (Pall). Tetramers were stored at 1 μM in 1× DPBS at 4°C prior to use. H3N2 X31-HA conjugated with APC and H3N2 Urg (Uruguay)-HA conjugated with PE were reported before [14].

Apoptosis analysis

Apoptosis of NP$_{311-325}$ T$_{RH}$, non-T$_{RH}$ cells or lung NP$_{366-374}$ T$_{RM}$, splenic NP$_{366-374}$ T$_{MEM}$ were assessed with CellEvent™ Caspase-3/7 Green Flow Cytometry Assay kit (ThermoFisher). Lung single cells were stained with surface markers then incubated with caspase 3/7 green detection reagent for 30 minutes at 37℃ as described in the manufacturer's instructions. Casepase 3/7 Flica activities were analyzed flow cytometry.

Immunohistochemistry and immunofluorescence

Left lobe of whole lungs was harvested and fixed in 10% formaldehyde (Fisher Scientific) until embedding. Fixed lung tissues were embedded in paraffin, sectioned at 10-μm thickness. To identify tertial lymphoid structure, the lung tissue slide was stained with hematoxylin and eosin by the Mayo Clinic Histology Core Laboratory (Scottsdale, AZ). To measured inducible bronchus-associated lymphoid tissues (iBALT) structure, lung tissue sections were deparaffinized in CitriSolv (Fisher Scientific) for 30 min and then immersed in ethanol series from 100, 95, 85, and 75% to distill H_2O for 5 min each for tissue hydration. For antigen retrieval, hydrated sections were steamed for 20 min in 1 mM EDTA (pH 8.0). For detecting, IL-21 expressing $CD4^+$ T cells in iBALT, left lobe of lungs from influenza infected-IL21-VFP reporter mice were harvested and fixed for overnight at room temperature in 4% paraformaldehyde (PFA). The tissues were incubated in 10% sucrose for overnight, then incubated in 30% sucrose before being embedded in OCT compound and cryosectioned. The frozen sections were fixed with cold acetone for 20 min. Lung sections were blocked with Super Block Blocking buffer (Fisher Scientific) for 1 hr at RT. Anti-B220-eflour660 (Clone: 4SM95, Invitrogen), -CD4-eflour570 (Clone: RA3-6B2, Invitrogen), -GL7-Alexa488 (Clone: GL7, Biolegend) and/or -GFP-Alexa488 (Clone: FM264G) were stained on the lung tissue sections for overnight at 4°C. After washing in 0.1% PBST (PBS with Tween 20), the slides were counterstained with 4', 6-diaminodino-2-phenylindole (DAPI) and mounted. Tissue staining was reviewed and representative images were acquired on a Zeiss LSM 780 confocal system (Carl Zeiss).

Quantitative RT-PCR

Total RNA was extracted from lung tissue or sorted cells as indicated in the text with Total RNA purification kit (Sigma) and treated with DNase I (Invitrogen). Random primers (Invitrogen) and MMLV reverse transcriptase (Invitrogen) were used to synthesize first-strand cDNAs from equivalent amounts of RNA from each sample. These cDNA was subjected to realtime-PCR with Fast SYBR Green PCR Master Mix (Applied Biosystems). Realtime-PCR was conducted in duplicates in QuantStudio3 (AppliedBioscience). Data were generated with the comparative threshold cycle (Delta CT) method by normalizing to hypoxanthine phosphoribosyltransferase (HPRT). Sequences of primers used in the studies are listed as following. *Hprt*-F:

CTCCGCCGGCTTCCTCCTCA, *Hprt*-R: ACCTGGTTCATCATCGCTAATC. *Il21*-F: CGCTCACGAATGCAGGAGTA, *Il21*-R: GTCTGTGCAGGGAACCACAA.

Parabiosis surgery

To examine tissue residency of lung T_{RH} or non-T_{RH} cells, parabiotic surgery was performed. CD45.1$^+$ or CD45.1$^+$/CD45.2$^+$ mice were infected with influenza PR8. 3 weeks later, mice were anesthetized with ketamine and xylazine and shaved in lateral skin area. After disinfection, shaved skin area was made an incision then matched from the olecranon to the knee joint of each mouse. Matching area was opposed with continuous sutures. Parabionts were then allowed to rest for 14 d before analysis. Equilibration of parabionts was confirmed in the peripheral blood before tissue analysis.

Nanostring analysis

To perform nanostring analysis, influenza-specific lung CD8 T_{RM}, splenic T_{MEM}, lung T_{RH}, lung non-T_{RH} and splenic T_{FH} cells were sorted as indicated in the text. Total RNA was extracted from sorted T cell populations with mini RNA-easy Kit (Qiagen). Equal amounts of total RNA from different groups were used for the assay. Hybridization reaction was established by following the instruction of the manufacturer. Aliquots of Reporter CodeSet and Capture ProbeSet were thawed at RT. Then, a master mix was created by adding 70 µl of hybridization buffer to the tube containing the reporter codeset. Eight microliters of this master mix was added to each of the tubes for different samples; 5 µl (50 ng) of the total RNA sample was added into each tube. Then, 2 µl of the well-mixed Capture probeset was added to each tube and placed in the preheated 65°C thermal cycler. All the sample mixes were incubated for 16 hours at 65°C for completion of hybridization. The samples were then loaded into the sample hole in the cartridge and loaded into the NanoString nCounter SPRINT Profiler machine (NanoString). When the corresponding Reporter Library File (RLF) running is finished, the raw data were downloaded and analyzed with NanoString Software nSolver 3.0 (NanoString). mRNA counts were processed to account for hybridization efficiency, background noise, and sample content, and were normalized using the geometric mean of housekeeping genes. All data were normalized by housekeeping genes. Heat map was generated by MeV software.

Single-cell RNA sequencing

Sorted $CD45_{i.v.}^{-}CD4^{+}CD44^{Hi}$ T cells from pooled lung cells of mice (5 mice) infected with influenza virus (28 d.p.i.) were loaded on the Chromium Controller (10x Genomics). Single-cell libraries were prepared using the Chromium Single Cell 3' Reagent kit (10x Genomics) following manufacturer's instruction. Paired-end sequencing was performed using an Illumina HiSeq 2500 in rapid-run mode. CellRanger software package (10x Genomics) were used to align and quantify sequencing data from 10x Genomics. All scRNA-seq analyses were performed in R using the package Seurat (version 2.0) [87].

Total RNA-sequencing

Lung $CD45_{i.v.}^{-}CD4^{+}CD44^{Hi}GITR^{-}PD\text{-}1^{Hi}FR4^{Hi}$, $CD45_{i.v.}^{-}CD4^{+}CD44^{Hi}GITR^{-}PD\text{-}1^{Low}FR4^{Low}$, splenic $CD4^{+}CD44^{Hi}GITR^{-}PD\text{-}1^{Hi}$ $CXCR5^{+}$ T_{FH} or splenic $CD4^{+}CD44^{Hi}GITR^{-}PD\text{-}1^{low}$ $CXCR5^{-}$ non-T_{FH} cells were sorted from total of 15 mice that were infected with influenza virus (28 d.p.i.). RNA was extracted using RNeasy Plus Mini Kit (Qiagen) following the manufacture's recommendation. After quality control, high quality (Agilent Bioanalyzer RIN >7.0) total RNA was used to generate the RNA sequencing library. cDNA synthesis, end-repair, A-base addition, and ligation of the Illumina indexed adapters were performed according to the TruSeq RNA Sample Prep Kit v2 (Illumina, San Diego, CA). The concentration and size distribution of the completed libraries was determined using an Agilent Bioanalyzer DNA 1000 chip (Santa Clara, CA) and Qubit fluorometry (Invitrogen, Carlsbad, CA). Paired-end libraries were sequenced on an Illumina HiSeq 4000 following Illumina's standard protocol using the Illumina cBot and HiSeq 3000/4000 PE Cluster Kit. Base-calling was performed using Illumina's RTA software (version 2.5.2). Paired-end RNA-seq reads were aligned to the mouse reference genome (GRCm38/mm10) using RNA-seq spliced read mapper Tophat2 (v2.1.1). Pre- and post-alignment quality controls, gene level raw read count and normalized read count (i.e. FPKM) were performed using RSeQC package (v2.3.6) with NCBI mouse RefSeq gene model. For functional analysis, GSEA was used to identify enriched gene sets, from the hallmark collection of MSigDB, having up-regulated and down-regulated genes, using a weighted enrichment statistic and a log2 ratio metric for ranking genes.

Quantification and Statistical Analysis

774 Statistical analysis was done using GraphPad Prism 7.0 (GraphPad Software) and presented as
775 means ± SEM. Unpaired or paired Student t tests and one-way or two-way ANOVA analysis
776 were used in data analysis. Logrank test was used for analysis of survival study.
777
778 **Acknowledgements**
779 We thank NIH tetramer core for tetramers and Mayo flow cytometry core for technical
780 assistance. We thank Genetech for α-CD20 and Drs. Barney Graham and Michelle Crank for
781 PR8 HA protein used in this study. This study was funded by the US National Institutes of
782 Health RO1s AI112844, AI147394 and AG047156 (J.S.), R01 AI125741 and RO1 AI148403
783 (W.C.) and R01 AI057459 (M.H.K.).
784
785
786
787
788
789
790
791
792
793
794
795
796
797
798
799
800
801
802
803

804 **Figure Legends:**

805 **Fig. 1 | Lung CD4$^+$ T cells deliver localized help for the development of tissue-resident B**
806 **and CD8$^+$ T cells.**

807 **a-e,** WT mice were infected with PR8 strain of influenza virus and treated with control (ctl) IgG
808 or α-CD4 starting at 14 d.p.i. Mice were injected with α-CD45 intravenously (i.v.) 5 min before
809 sacrifice at 42 d.p.i. **a**, Experimental scheme. **b**, Representative confocal images of iBALT in the
810 lung. Lung sections were stained with α-CD4 (red), α-B220 (green) and DAPI (blue). **c,**
811 Frequencies and cell number of influenza HA-specific B cells (HA-B) in the lung tissue
812 ($CD45_{i.v.}^-B220^+GL7^-HA^+$), lung blood vessels ($CD45_{i.v.}^+B220^+GL7^-HA^+$) and spleen
813 ($B220^+GL7^-HA^+$). **d,** Lung tissue $CD8^+$, $CD8^+CD69^+$ or $CD8^+CD69^+CD103^+$ $NP_{366-374}$ or PA_{224-}
814 $_{233}$ T_{RM} cells were enumerated. **e,** Splenic $CD8^+$ $NP_{366-374}$ or $PA_{224-233}$ memory cells ($T_{MEM-SPL}$)
815 were enumerated. **f-j,** WT mice were infected with PR8 and treated with ctrl IgG or α-CD4
816 (starting at 14 d.p.i.) in the presence of daily injection of FTY-720 (starting at 13 d.p.i.). **f**,
817 Schematic of experimental design. **g**, B_{GC} cell numbers were enumerated by flow cytometry. **h**, **i,**
818 Total HA-specific B cells (total HA-B) (**h**) or HA-specific tissue-resident memory B cells (HA-
819 B_{RM}: $CD45_{i.v.}^-B220^+GL7^-IgD^-IgM^-HA^+CD38^+$) (**i**) were enumerated. **j**, Lung tissue $CD8^+$,
820 $CD8^+CD69^+$ or $CD8^+CD69^+CD103^+$ $NP_{366-374}$ or $PA_{224-233}$ T_{RM} cells were enumerated. **k-n,** WT
821 mice were infected with PR8 and received ctl IgG, high or low dose of α-CD4. Cell number of
822 B_{GC} (**k**), HA-specific B_{RM} (**l**) and NP-specific B_{RM} cells (**m**) in the lung tissue. **n,** Lung tissue
823 $CD8^+$, $CD8^+CD69^+$ or $CD8^+CD69^+CD103^+$ $NP_{366-374}$ T_{RM} cells were enumerated. In **b-e** were the
824 representative data from at least two independent experiments (4-5 mice per group). In **g-h and**
825 **j-n**, data were pooled from two (**g**, **h** and **j**) or three (**k-n**) independent experiments (2-5 mice per
826 group). *P* values were calculated by unpaired two-tailed Student's t-test in c-j. *P* values in k-n
827 were analyzed by one-way ANOVA.

828

829 **Fig. 2 | Identification of a population of T_{FH}-like cells in the lung tissue.**

830 WT (**a-e**) or IL-21-VFP reporter (**f**) mice were infected with PR8. **a**, tSNE plot of scRNAseq
831 analysis of sorted lung $CD45_{i.v.}^-CD4^+CD44^{Hi}$ cells (pooled from 5 mice) at 28 d.p.i. **b**, Heat map
832 of indicated genes in each cluster from scRNAseq data. **c**, Kinetics of the percentages of PD-
833 $1^{Hi}FR4^{Hi}$ population in lung tissue total $CD4^+$ or influenza NP-specific ($NP_{311-325}$) $CD4^+$ T cells.
834 **d**, Expression of T_{FH} cell-associated markers in lung total or influenza-specific PD-$1^{Hi}FR4^{Hi}$, PD-

835 $1^{Low}FR4^{Low}$ or splenic T_{FH} ($CD4^+CD44^{Hi}PD\text{-}1^+CXCR5^+$) cells at 28 d.p.i. **e**, Expression of IFN-γ,
836 IL-17 or IL-4 by lung PD-$1^{Hi}FR4^{Hi}$, PD-$1^{Low}FR4^{Low}$ or spleen T_{FH} cells were identified by
837 intracellular staining at 28 d.p.i**. f**, IL-21-VFP expression in lung $CD4^+$ PD-$1^{Hi}FR4^{Hi}$, PD-
838 $1^{Low}FR4^{Low}$ or spleen T_{FH} at 28 d.p.i. In **c-f**, representative plots, histograms and graphs were
839 from at least two independent experiments (4 mice per group). *P* values in e and f were analyzed
840 by one-way ANOVA.
841
842
843 **Fig. 3 | Transcriptional profiling reveals PD-$1^{Hi}FR4^{Hi}$ cells exhibit both T_{FH} and T_{RM} gene**
844 **signatures.**
845 **a-f**, WT mice were infected with PR8. Lung PD-$1^{Hi}FR4^{Hi}$ or PD-$1^{Low}FR4^{Low}$ $CD4^+$ T cells and
846 splenic T_{FH} or non-T_{FH} cells were sorted following exclusion of $GITR^{Hi}$ Treg cells and RNA-seq
847 analysis was performed at 28 d.p.i. **a**, Heatmap expression of differentially expressed genes
848 among lung PD-$1^{Hi}FR4^{Hi}$, PD-$1^{Low}FR4^{Low}$ $CD4^+$ T cells and splenic T_{FH} or non-T_{FH} cells. **b**,
849 Principle component analysis of RNA-seq data of lung PD-$1^{Hi}FR4^{Hi}$, PD-$1^{Low}FR4^{Low}$ $CD4^+$ T
850 cells and splenic T_{FH} or non-T_{FH} cells. **c,** Volcano plot of RNA-seq analysis of lung PD-$1^{Hi}FR4^{Hi}$
851 or PD-$1^{Low}FR4^{Low}$ $CD4^+$ T cells. **d**, GSEA of the core T_{FH} signature genes in lung $CD4^+$ PD-
852 $1^{Hi}FR4^{Hi}$ and $CD4^+$ PD-$1^{Low}FR4^{Low}$ cells. **e**, Volcano plot of RNA-seq analysis on lung PD-1^{Hi}
853 $FR4^{Hi}$ $CD4^+$ T and splenic T_{FH} cells. **f**, GSEA of the core tissue-residency signature genes of T_{RM}
854 cells in lung PD-$1^{Hi}FR4^{Hi}$ and splenic T_{FH} cells. **g-h,** WT mice were infected with PR8. Lung
855 PD-$1^{Hi}FR4^{Hi}$ or PD-$1^{Low}FR4^{Low}$ $CD4^+$ T cells and splenic T_{FH} cells were sorted at 28 d.p.i.
856 Nanostring analysis on 560 immune-associated genes was performed. The expression of T_{FH}-
857 associated genes (**g**) or tissue-residency associated genes (**h**) in the three cell populations was
858 depicted. For RNA-seq, data were from duplicates of pooled samples (n = 15). For nanostring
859 analysis, data were from pooled samples (n = 10).
860
861 **Fig. 4 | Lung PD-$1^{Hi}FR4^{Hi}$ cells are tissue resident**
862 **a**, WT mice were infected with PR8. The expression of CD69, CXCR6 and *Bhlhe40* in lung
863 $CD4^+$ PD-$1^{Hi}FR4^{Hi}$ or $CD4^+$ PD-$1^{Low}FR4^{Low}$ $NP_{311\text{-}325}$ T cells or splenic T_{FH} cells at 28 d.p.i. **b-e**,
864 $CD45.1^+$ (Host) or $CD45.1^+$ $CD45.2^+$ (Partner) WT mice were infected with PR8. Parabiosis
865 surgery was performed at 21 d.p.i. Mice were sacrificed 14 days later for analysis. **b,** Schematics

of parabiosis experiments. **c**, Composition of Host-derived or Partner-derived $CD4^+$ T cells in the spleens of the parabionts. **d**, Frequencies of Host-derived or Partner-derived cells in the lung PD-$1^{Hi}FR4^{Hi}$ or PD-$1^{Low}FR4^{Low}$ total $CD4^+$ T cell compartment. **e**, Frequencies of Host-derived or Partner-derived cells in influenza-specific lung $CD4^+$ PD-$1^{Hi}FR4^{Hi}$ or $CD4^+$ PD-$1^{Low}FR4^{Low}$ $NP_{311-325}$ T cell compartment. In **a**, the representative histograms were from at least two independent experiments (3-4 mice per group). Parabiosis data were pooled from two different experiments (two pairs per experiment). *P* values in d and e were analyzed by one-way ANOVA.

Fig. 5 | Optimal T_{RH} formation requires lung B cells and iBALT formation

WT (**a-d**) mice were infected with PR8 and treated with ctl IgG, α-CD20 (**b**) or LTβR-Ig (**c** and **d**) (weekly starting at 14 d.p.i.) in the presence of daily injection of FTY-720 (13-27 d.p.i.). **a**, Experimental scheme. **b** and **d,** Representative dot plot and cell numbers of influenza-specific $NP_{311-325}$ lung $T_{RH,}$ lung non-T_{RH} or splenic T_{FH} cells. **c,** Representative image from lung tissue section stained with B220/GL-7 following ctl IgG or LTβR-Ig treatment. In **c**, the representative image was from at least two independent experiments (3-4 mice per group). In **b,** representative data were from at least two independent experiments (4-5 mice per group). In **d**, data were pooled from two independent experiments (3-4 mice per group). *P* values were calculated by unpaired two-tailed Student's t-test.

Fig. 6 | Both BCL6 and Bhlhe40 are required for optimal lung T_{RH} responses.

a-e, *Bcl6*$^{fl/fl}$ or *Bcl6*$^{\Delta T}$ mice were infected with PR8. Representative dot plot (**a**), percentages (**b**) and cell numbers (**c**) of T_{RH} or non-T_{RH} in lung $CD45_{i.v.}^-$ total $CD4^+$ or $CD45_{i.v.}^-$ influenza-specific $CD4^+$ $NP_{311-325}$ T cells at 28 d.p.i. **d-e**, Representative dot plot (**d**) and percentage (top row) or cell numbers (bottom row) (**e**) of splenic total T_{FH} or $NP_{311-325}$ T_{FH} at 28 d.p.i. **f**, GSEA of the *Bhlhe40*-associated genes in lung T_{RH} (PD-$1^{Hi}FR4^{Hi}$) and spleen T_{FH} cells. **g-k**, *Bhlhe40*$^{fl/fl}$ or *Bhlhe40*$^{\Delta T}$ mice were infected with PR8. **g-i**, Representative dot plot (**g**)**,** percentages (**h**) or cell numbers (**i**) of influenza-specific $NP_{311-325}$ lung T_{RH}, lung non-T_{RH}, splenic T_{FH} or splenic non-T_{FH} cells at 28 d.p.i. **j-k** Representative dot plot (**j**) or percentages (**k**) of active caspase 3/7-$FLICA^+$ cells in lung $NP_{311-325}$ T_{RH} or non-T_{RH} cells at 28 d.p.i. In **a-e** and **g-i**, data were pooled from two independent experiments (3-4 mice per group). In **j-k**, representative data were from at

least two independent experiments (4 mice per group). *P* values were calculated by unpaired two-tailed Student's t-test.

Fig. 7 | T_{RH} cells are required for the development of lung protective $CD8^+$ T_{RM} and B cell immunity.

a-j, *Bcl6*$^{fl/fl}$ or *Bcl6*$^{\Delta CD4ERT2}$ mice were infected with PR8. **a-e,** Tamoxifen was administrated daily from 12-16 d.p.i. in the presence of daily FTY720 administration (11-34 d.p.i.). **a**, Schematics of experimental design. Cell numbers of B_{GC} (**b**), HA-specific B_{RM} (**c**), NP-specific B_{RM} (**d**), **e**, $CD8^+CD69^+$ $NP_{366-374}$ T_{RM} or $CD8^+CD69^+$ $PA_{224-233}$ T_{RM} at 35 d.p.i. **f-j**, Tamoxifen was administrated daily from 21-25 d.p.i. in the presence of daily FTY720 administration (20-41 d.p.i.). **f**, Schematics of experimental design. Cell numbers of B_{GC} (**g**), HA-specific B_{RM} (**h**), NP-specific B_{RM} (**i**), **j**, $CD8^+CD69^+$ $NP_{366-374}$ T_{RM} or $CD8^+CD69^+$ $PA_{224-233}$ T_{RM} at 42 d.p.i. **k**, *Bcl6*$^{fl/fl}$ or *Bcl6*$^{\Delta CD4ERT2}$ mice were infected with X31 strain (H3N2) of influenza. Tamoxifen was administrated daily from 12-16 d.p.i. in the presence of daily FTY720 administration (11-34 d.p.i.). Representative dot plot (top) and cell numbers (bottom) of X31 strain-specific B_{RM} or cross-reactive HA-specific B_{RM} (to H3N2 A/Uruguay/716/07 strain) at 35 d.p.i. **l-m**, *Bcl6*$^{fl/fl}$ (n = 11) or *Bcl6*$^{\Delta CD4ERT2}$ (n = 15) mice were infected with X31 and administered with tamoxifen from 12 to 16 d.p.i. Mice were re-challenged with PR8 at 42 d.p.i. in the presence of FTY720 (starting from 41d). **l**, Schematics of experimental design. **m**, Host mortality following PR8 challenge was monitored. In **a-h and j-k**, all data were pooled from two (**c**, **d**, **k,** **g**, **h** and **j**) or three (**b** and **e**) independent experiments (2-5 mice per group). In a-k, *P* values were calculated by unpaired two-tailed Student's t-test. *P* value of survival study in m was calculated by Logrank test.

Fig. 8 | IL-21 or CD40L-dependent T_{RH} help to $CD8^+$ or B cells.

a-b, IL-21-VFP reporter mice were infected with PR8. **a,** IL-21-VFP expressing cells in the lungs or spleens were identified by flow cytometry at 28 d.p.i. **b**, Representative dot plot of IL-21^{Hi} or IL-21^{Low} $CD4^+$ T cells that were PD-1^{Hi}FR4^{Hi}. **c-f,** WT mice were infected PR8 with or without IL-21R blockade through intraperitoneal (I.P.) route starting at 14 d.p.i. in the presence of FTY-720 administration (13-34 d.p.i.). **c,** Experimental scheme. Cell numbers of lung parenchymal B_{GC} (**d**), HA-specific B_{RM} (**e**) and $CD8^+CD69^+$ $NP_{366-374}$ or $CD8^+CD69^+$ $PA_{224-233}$ T_{RM} cells (**f**). **g-k**, WT mice were infected with PR8 with or without IL-21R blockade through

intranasal (I.N.) route at 14 d.p.i. **g**, Experimental scheme. **h-i**, Frequencies (**h**) or cell numbers (**i**) of lung tissue $CD8^+CD69^+$ $NP_{366-374}$, $CD8^+CD69^+$ $PA_{224-233}$ T_{RM}, splenic $CD8^+$ $NP_{366-374}$ or $PA_{224-233}$ memory T cells (T_{MEM}) at 42 d.p.i. **j,** Percentage of apoptotic cells were identified by active caspase 3/7-FLICA staining within lung $CD8^+$ $NP_{366-374}$ T_{RM} or splenic $CD8^+$ $NP_{366-374}$ T_{MEM} at 28 d.p.i. **k**, percentages of proliferating cells were identified by Ki67 staining within lung $CD8^+$ $NP_{366-374}$ T_{RM} or splenic $CD8^+$ $NP_{366-374}$ T_{MEM} at 28 d.p.i. **l**, Representative histogram of BATF expression in lung $CD8^+$ $NP_{366-374}$ or $CD8^+$ $PA_{224-233}$ T_{RM} of mice received with ctl IgG or α-IL21R at 35 d.p.i. **m**, Representative histogram of CD40L expression in influenza-specific lung T_{RH} or non-T_{RH} at 28 d.p.i. **n-o,** WT mice were infected with PR8 and received ctl IgG or α-CD40L weekly (I.P. route) starting at 14 d.p.i. in the presence of daily FTY-720 administration (13-34 d.p.i.). Representative dot plot or cell numbers B_{GC} (**n**) and HA-specific B_{RM} (**o**) cells at 35 d.p.i. In **a-b and j-m**, representative data were from at least two independent experiments (4-5 mice per group). In **d, f-i** and **n-o**, data were pooled from two independent experiments (3-5 mice per group). *P* values of all experiments were calculated by unpaired two-tailed Student's t-test.

Extended Fig. 1 | "Late" $CD4^+$ T cell help shapes respiratory mucosal memory $CD8^+$ and B cell immunity.

WT mice were infected with PR8 and treated with ctl IgG or α-CD4. **a,** The efficiency of $CD4^+$ T cell depletion in the lung or spleen. **b**, Representative image of lung section stained with H&E. Black arrows indicate tertial lymphoid structure. **c**, Representative dot plot and cell numbers of lung germinal center B (B_{GC}) cells. **d**, Frequencies of lung circulating ($CD45_{i.v.}^+$) or parenchymal ($CD45_{i.v.}^-$) $CD8^+$ T or B cells in mice treated with control IgG or α-CD4. **e**, Influenza HA-specific B cells (HA-B) in the lungs were identified through HA antigen staining. **f**, Lung tissue or circulating $CD8^+$ $NP_{366-374}$ or $PA_{224-233}$ T cells were identified through $CD45_{i.v.}$ staining and analyzed by flow cytometry. **g,** Lung circulating $CD8^+$ $NP_{366-374}$ or $CD8^+$ $PA_{224-233}$ T cells were enumerated. **i,** Histogram of CD103 expression or frequency of $CD103^+$ cells within $CD8^+CD69^+$ $NP_{366-374}$ T_{RM} cells. **h, j,** Gating strategies of $CD8^+$ T_{RM} (**h**) or B_{RM} (**j**) cells in the lung. Representative data were from at least two independent experiments (4-5 mice per group). *P* values were calculated by unpaired two-tailed Student's t-test.

Extended Fig. 2 | Lung "local" CD4 T cell help for the development robust memory $CD8^+$ and B cell immunity.

WT mice were infected with influenza PR8 (**a**) or X31 (**b-e**) and treated with control IgG or α-CD4 (starting at 14 d.p.i.) in the presence of daily FTY720 (starting at 13 d.p.i.).

a, Blood lymphocytes in the PBS or FTY720 administrated mice. **b-e**, Numbers of lung B_{GC} cells (**b**), total HA specific B cells (**c**), HA-specific B_{RM} (**d**), and total $CD8^+$ $NP_{366-374}$ memory T cells, $CD8^+$ $CD69^+$ $NP_{366-374}$ T_{RM} or $CD8^+$ $CD69^+$ $CD103^+$ $NP_{366-374}$ T_{RM} cells (**e**). **f-h**, WT mice were infected with PR8 and received with ctl IgG, low or high dose of α-CD4 (starting at 14 d.p.i.). Experimental scheme (**f**), representative dot plot of blood lymphocyte population (**g**) and lung lymphocyte population (**h**). Representative data were from at least two independent experiments (4-5 mice per group). *P* values were calculated by unpaired two-tailed Student's t-test.

Extended Fig. 3 | scRNA-seq identifies a population of lung T_H cells exhibit T_{FH} features.

a, Heat map of signature genes following high-rank cluster analysis of scRNAseq data. **b**, 5 clusters of lung T helper cells were identified following scRNA seq analysis. **c**, Violin plot of representative T_H genes in each cluster.

Extended Fig. 4 | Total RNA-seq identified PD-$1^{Hi}$$FR4^{Hi}$ cells exhibits features of T_{FH} and T_{RM}.

a, Cell sorting strategy for lung PD-$1^{Hi}$$FR4^{Hi}$, PD-$1^{Low}$$FR4^{Low}$ population in the lungs. To exclude $Foxp3^+$ T_{reg} cells, lung PD-$1^{Hi}$$FR4^{Hi}$, PD-$1^{Low}$$FR4^{Low}$ cells were sorted from $CD45_{i.v.}^-CD4^+GITR^-$ $CD44^{Hi}$ population. **b**, Cluster analysis of signature genes in lung PD-$1^{Hi}$$FR4^{Hi}$, lung PD-$1^{Low}$$FR4^{Low}$, splenic T_{FH} or splenic non-T_{FH} cells. **c**, GSEA of lung PD-$1^{Hi}$$FR4^{Hi}$ and lung PD-$1^{Low}$$FR4^{Low}$ cells. **d**, GSEA of lung PD-$1^{Hi}$$FR4^{Hi}$ and splenic T_{FH} cells.

Extended Fig. 5 | Impaired T_{RH} responses following B cell depletion, iBALT disruption or Bhlhe40 deficiency.

a-c, WT (**a** and **c**) or IL-21-VFP reporter (**b**) mice were infected with PR8 and received with ctl IgG, α-CD20 or LTβR-Ig weekly in the present of FTY-720 (Experimental scheme in Fig 5. a.).

a, The efficiency of B cell depletion in the lung. **b**, Representative confocal images of IL-21-

989 expressing cells in iBALT. **c**, Cell numbers of lung tissue B cells in mice received with ctl-IgG
990 or LTβR-Ig. **d-g**, *Bhlhe40*$^{fl/fl}$ or *Bhlhe40*$^{\Delta T}$ mice were infected with PR8. Representative dot plot
991 (**d**), percentages (top) or cell numbers (bottom) (**e**) of total lung T_{RH}, non-T_{RH}, splenic T_{FH} or
992 splenic non-T_{FH} at 28 d.p.i. **f,** Representative dot plot or cell numbers of lung tissue or splenic
993 $CD4^+$ T cells at 28 d.p.i. **g,** Cell numbers of lung or splenic influenza-$NP_{311-325}$ $CD4^+$ T cell at 28
994 d.p.i. Data were pooled from two independent experiments (3-4 mice per group). *P* value were
995 calculated by unpaired two-tailed Student's t-test.
996
997 **Extended Fig. 6 | T cell-specific BCL6 or Bhlhe40 deficiency leads to impaired lung $CD8^+$**
998 **memory and B cell immunity.**
999 **a-d**, *Bcl6*$^{fl/fl}$ or *Bcl6*$^{\Delta T}$ mice were infected with PR8. **a,** Representative confocal images of lung
1000 iBALT at 28 d.p.i. Lung sections were stained with α-CD4 (red), α-B220 (green), α-GL7 (white)
1001 and DAPI (blue). Percentages of lung B_{GC} (**b**), lung tissue HA-specific B_{RM} or circulating HA-
1002 specific B_{MEM} (**c**) and $CD8^+CD69^+$ $NP_{366-374,}$ or $CD8^+CD69^+$ $PA_{224-233}$ T_{RM} (**d**). **e-g,** *Bhlhe40*$^{fl/fl}$ or
1003 *Bhlhe40*$^{\Delta T}$ mice were infected with PR8. **e,** Representative dot plot or cell numbers of lung tissue
1004 $CD8^+$ T (top) or B cells (bottom) at 28 d.p.i. **f,** Cell numbers of NP-specific B_{RM} or HA-specific
1005 B_{RM} cells. **g,** Cell numbers of $CD8^+CD69^+$ $NP_{366-374,}$ or $CD8^+CD69^+$ $PA_{224-233}$ $T_{RM.}$. In **a-d** and **f-**
1006 **g**, representative data were from at least two independent experiments (4-5 mice per group). In **e**,
1007 data were pooled from two independent experiments (4 mice per group). *P* values of all
1008 experiments were calculated by unpaired two-tailed Student's t-test.
1009
1010 **Extended Fig. 7 | T_{RH} cells help local development of memory $CD8^+$ and B cells.**
1011 **a-c**, *Bcl6*$^{fl/fl}$ (with ROSA26 LSL-YFP transgene) or *Bcl6*$^{\Delta CD4ERT2}$ (with ROSA26 LSL-YFP
1012 transgene) mice were infected with X31. Tamoxifen was administrated daily from 12 to 16 d.p.i.
1013 **a,** Experimental scheme of selective deletion of *Bcl6* in $CD4^+$ T cells. **b**, **c,** YFP expression in
1014 blood $CD45^+$ (**b**) or $CD4^+$ T (**c**) cells following tamoxifen injection. **d, e,** *Bcl6*$^{fl/fl}$ or *Bcl6*$^{\Delta CD4ERT2}$
1015 mice were infected with PR8. Tamoxifen was administrated daily from 12-16 d.p.i. in the
1016 presence of daily FTY720 administration (11-34 d.p.i.). **d**, Cell numbers of $CD45_{i.v.}^-$ $CD4^+$ T,
1017 $CD8^+$ T or B cells at 35 d.p.i. **e**, Representative dot plot (top) or cell numbers (bottom) of $NP_{311-325}$ T_{RH} or non-T_{RH} cells at 35 d.p.i. **f**, Cell numbers of lung $CD8^+CD69^+$ $NP_{366-374}$ or $CD8^+CD69^+$
1019 $PA_{224-233}$ T_{RM}, B_{GC} or HA-specific B_{RM} cells were enumerated from X31-infected *Bcl6*$^{fl/fl}$ and

Bcl6$^{\Delta CD4ERT2}$ mice in the present of FTY720 (11-34 d.p.i.) at 35 d.p.i. In **a-c** and **f**, representative data were from at least two independent experiments (2-5 mice per group). In **d-e**, data were pooled from two independent experiments (3 mice per group). *P* values of all experiments were calculated by unpaired two-tailed Student's t-test.

Extended Fig. 8 | T_{RH} cells help $CD8^+$ T and B cells through IL-21 or CD40L dependent mechanisms.

a, Expression of *Il21* gene in sorted IL-21-$VFP^{Hi,}$ IL-21-VFP^{Low} or IL-21-VFP^- $CD4^+$ T cells from the lung tissue at 21 d.p.i. (pooled from 8 mice) **b**, Expression of *Il21* in the whole lung from *Bcl6*$^{fl/fl}$ or *Bcl6*$^{\Delta T}$ mice at 15 or 42 d.p.i. **c,** Frequencies or cell numbers of lung B_{GC} or HA-specific B cells from PR8 infected WT mice treated with ctl-IgG or α-IL-21R (Intranasal route). **d**, Heat map of IL-21 signaling-related genes from sorted lung $CD8^+$ $NP_{366-374}$ or $PA_{224-233}$ T_{RM} or splenic $CD8^+$ $NP_{366-374}$ or $PA_{224-233}$ T_{MEM} determined by Nanostring at 38 d.p.i. as reported previously [40]. **e,** Geometric M.F.I. of BATF expression in lung $CD8^+$ $NP_{366-374,}$ $CD8^+$ $PA_{224-233}$ T_{RM}, splenic $CD8^+$ $NP_{366-374}$ or $PA_{224-233}$ T_{MEM} cells from PR8 infected mice at 35 d.p.i. **f,** CD40L expression in the $NP_{311-325}$ T_{RH} or non-T_{RH} cells following PMA/Ionomycin stimulation at 28 d.p.i. **g,** Schematics of the summary. In **b-c** and **e-f**, representative data were from at least two independent experiments (3-5 mice per group). *P* values were calculated by unpaired (b and c) or paired (f) two-tailed Student's t-test. *P* value in e was analyzed by one-way ANOVA.

References

1. Onodera, T. *et al.* Memory B cells in the lung participate in protective humoral immune responses to pulmonary influenza virus reinfection. *Proc Natl Acad Sci U S A* **109**, 2485-2490 (2012).

2. Schenkel, J.M. & Masopust, D. Tissue-resident memory T cells. *Immunity* **41**, 886-897 (2014).

3. Mueller, S.N. & Mackay, L.K. Tissue-resident memory T cells: local specialists in immune defence. *Nat Rev Immunol* **16**, 79-89 (2016).

4. Milner, J.J. & Goldrath, A.W. Transcriptional programming of tissue-resident memory CD8(+) T cells. *Curr Opin Immunol* **51**, 162-169 (2018).

5. Allie, S.R. *et al.* The establishment of resident memory B cells in the lung requires local antigen encounter. *Nat Immunol* **20**, 97-108 (2019).

6. Park, S.L. *et al.* Local proliferation maintains a stable pool of tissue-resident memory T cells after antiviral recall responses. *Nat Immunol* **19**, 183-191 (2018).

7. Beura, L.K. *et al.* Intravital mucosal imaging of CD8(+) resident memory T cells shows tissue-autonomous recall responses that amplify secondary memory. *Nat Immunol* **19**, 173-182 (2018).

8. Jameson, S.C. & Masopust, D. Understanding Subset Diversity in T Cell Memory. *Immunity* **48**, 214-226 (2018).

9. Ruf, B.R. & Knuf, M. The burden of seasonal and pandemic influenza in infants and children. *Eur J Pediatr* **173**, 265-276 (2014).

10. Molinari, N.A. *et al.* The annual impact of seasonal influenza in the US: measuring disease burden and costs. *Vaccine* **25**, 5086-5096 (2007).

11. Rolfes, M.A. *et al.* Annual estimates of the burden of seasonal influenza in the United States: A tool for strengthening influenza surveillance and preparedness. *Influenza Other Respir Viruses* **12**, 132-137 (2018).

12. Turner, D.L. *et al.* Lung niches for the generation and maintenance of tissue-resident memory T cells. *Mucosal Immunol* **7**, 501-510 (2014).

13. Takamura, S. & Kohlmeier, J.E. Establishment and Maintenance of Conventional and Circulation-Driven Lung-Resident Memory CD8(+) T Cells Following Respiratory Virus Infections. *Front Immunol* **10**, 733 (2019).

14. Adachi, Y. *et al.* Distinct germinal center selection at local sites shapes memory B cell response to viral escape. *J Exp Med* **212**, 1709-1723 (2015).

15. Sun, J. & Braciale, T.J. Role of T cell immunity in recovery from influenza virus infection. *Curr Opin Virol* **3**, 425-429 (2013).

16. La Gruta, N.L. & Turner, S.J. T cell mediated immunity to influenza: mechanisms of viral control. *Trends Immunol* **35**, 396-402 (2014).

17. Duan, S. & Thomas, P.G. Balancing Immune Protection and Immune Pathology by CD8(+) T-Cell Responses to Influenza Infection. *Front Immunol* **7**, 25 (2016).

18. Kohlmeier, J.E. & Woodland, D.L. Immunity to respiratory viruses. *Annu Rev Immunol* **27**, 61-82 (2009).

19. Wilkinson, T.M. *et al.* Preexisting influenza-specific CD4+ T cells correlate with disease protection against influenza challenge in humans. *Nat Med* **18**, 274-280 (2012).

20. Sridhar, S. *et al.* Cellular immune correlates of protection against symptomatic pandemic influenza. *Nat Med* **19**, 1305-1312 (2013).

21. McMaster, S.R., Wilson, J.J., Wang, H. & Kohlmeier, J.E. Airway-Resident Memory CD8 T Cells Provide Antigen-Specific Protection against Respiratory Virus Challenge through Rapid IFN-gamma Production. *J Immunol* **195**, 203-209 (2015).

22. Pizzolla, A. & Wakim, L.M. Memory T Cell Dynamics in the Lung during Influenza Virus Infection. *J Immunol* **202**, 374-381 (2019).

23. Koutsakos, M. *et al.* Human CD8(+) T cell cross-reactivity across influenza A, B and C viruses. *Nat Immunol* (2019).

24. Pizzolla, A. *et al.* Influenza-specific lung-resident memory T cells are proliferative and polyfunctional and maintain diverse TCR profiles. *J Clin Invest* **128**, 721-733 (2018).

25. Slutter, B. *et al.* Dynamics of influenza-induced lung-resident memory T cells underlie waning heterosubtypic immunity. *Sci Immunol* **2** (2017).

26. Cauley, L.S. Environmental cues orchestrate regional immune surveillance and protection by pulmonary CTLs. *J Leukoc Biol* **100**, 905-912 (2016).

27. Johnson, S. *et al.* Selected Toll-like receptor ligands and viruses promote helper-independent cytotoxic T cell priming by upregulating CD40L on dendritic cells. *Immunity* **30**, 218-227 (2009).

28. Sun, J., Dodd, H., Moser, E.K., Sharma, R. & Braciale, T.J. CD4+ T cell help and innate-derived IL-27 induce Blimp-1-dependent IL-10 production by antiviral CTLs. *Nat Immunol* **12**, 327-334 (2011).

29. Belz, G.T., Wodarz, D., Diaz, G., Nowak, M.A. & Doherty, P.C. Compromised influenza virus-specific CD8(+)-T-cell memory in CD4(+)-T-cell-deficient mice. *J Virol* **76**, 12388-12393 (2002).

30. Laidlaw, B.J. *et al.* CD4+ T cell help guides formation of CD103+ lung-resident memory CD8+ T cells during influenza viral infection. *Immunity* **41**, 633-645 (2014).

31. Crotty, S. A brief history of T cell help to B cells. *Nat Rev Immunol* **15**, 185-189 (2015).

32. Papillion, A. *et al.* Inhibition of IL-2 responsiveness by IL-6 is required for the generation of GC-TFH cells. *Sci Immunol* **4** (2019).

33. Allie, S.R. & Randall, T.D. Pulmonary immunity to viruses. *Clin Sci (Lond)* **131**, 1737-1762 (2017).

34. Rao, D.A. *et al.* Pathologically expanded peripheral T helper cell subset drives B cells in rheumatoid arthritis. *Nature* **542**, 110-114 (2017).

35. Rao, D.A. T Cells That Help B Cells in Chronically Inflamed Tissues. *Front Immunol* **9**, 1924 (2018).

36. Vu Van, D. *et al.* Local T/B cooperation in inflamed tissues is supported by T follicular helper-like cells. *Nat Commun* **7**, 10875 (2016).

37. Tan, H.X. *et al.* Inducible Bronchus-Associated Lymphoid Tissues (iBALT) Serve as Sites of B Cell Selection and Maturation Following Influenza Infection in Mice. *Front Immunol* **10**, 611 (2019).

38. Hornick, E.E., Zacharias, Z.R. & Legge, K.L. Kinetics and Phenotype of the CD4 T Cell Response to Influenza Virus Infections. *Front Immunol* **10**, 2351 (2019).

39. Woodland, D.L. & Kohlmeier, J.E. Migration, maintenance and recall of memory T cells in peripheral tissues. *Nat Rev Immunol* **9**, 153-161 (2009).

40. Wang, Z. *et al.* PD-1(hi) CD8(+) resident memory T cells balance immunity and fibrotic sequelae. *Sci Immunol* **4** (2019).

41. Hufford, M.M., Kim, T.S., Sun, J. & Braciale, T.J. Antiviral CD8+ T cell effector activities in situ are regulated by target cell type. *J Exp Med* **208**, 167-180 (2011).

42. Sun, J., Madan, R., Karp, C.L. & Braciale, T.J. Effector T cells control lung inflammation during acute influenza virus infection by producing IL-10. *Nat Med* **15**, 277-284 (2009).

43. Yao, S. *et al.* Interferon regulatory factor 4 sustains CD8(+) T cell expansion and effector differentiation. *Immunity* **39**, 833-845 (2013).

44. Anderson, K.G. *et al.* Intravascular staining for discrimination of vascular and tissue leukocytes. *Nat Protoc* **9**, 209-222 (2014).

45. Goplen, N.P. *et al.* Tissue-Resident Macrophages Limit Pulmonary CD8 Resident Memory T Cell Establishment. *Front Immunol* **10**, 2332 (2019).

46. Moyron-Quiroz, J.E. *et al.* Role of inducible bronchus associated lymphoid tissue (iBALT) in respiratory immunity. *Nat Med* **10**, 927-934 (2004).

47. Hwang, J.Y., Randall, T.D. & Silva-Sanchez, A. Inducible Bronchus-Associated Lymphoid Tissue: Taming Inflammation in the Lung. *Front Immunol* **7**, 258 (2016).

48. Thomas, P.G., Keating, R., Hulse-Post, D.J. & Doherty, P.C. Cell-mediated protection in influenza infection. *Emerg Infect Dis* **12**, 48-54 (2006).

49. La Gruta, N.L. *et al.* A virus-specific CD8+ T cell immunodominance hierarchy determined by antigen dose and precursor frequencies. *Proc Natl Acad Sci U S A* **103**, 994-999 (2006).

50. Ballesteros-Tato, A., Leon, B., Lee, B.O., Lund, F.E. & Randall, T.D. Epitope-specific regulation of memory programming by differential duration of antigen presentation to influenza-specific CD8(+) T cells. *Immunity* **41**, 127-140 (2014).

51. Baeyens, A., Fang, V., Chen, C. & Schwab, S.R. Exit Strategies: S1P Signaling and T Cell Migration. *Trends Immunol* **36**, 778-787 (2015).

52. Marnik, E.A. *et al.* Precocious Interleukin 21 Expression in Naive Mice Identifies a Natural Helper Cell Population in Autoimmune Disease. *Cell Rep* **21**, 208-221 (2017).

53. Wu, T. *et al.* TCF1 Is Required for the T Follicular Helper Cell Response to Viral Infection. *Cell Rep* **12**, 2099-2110 (2015).

54. Kumar, B.V. *et al.* Human Tissue-Resident Memory T Cells Are Defined by Core Transcriptional and Functional Signatures in Lymphoid and Mucosal Sites. *Cell Rep* **20**, 2921-2934 (2017).

55. Li, C. *et al.* The Transcription Factor Bhlhe40 Programs Mitochondrial Regulation of Resident CD8(+) T Cell Fitness and Functionality. *Immunity* **51**, 491-507 e497 (2019).

56. Beura, L.K. *et al.* CD4(+) resident memory T cells dominate immunosurveillance and orchestrate local recall responses. *J Exp Med* **216**, 1214-1229 (2019).

57. Crotty, S. T Follicular Helper Cell Biology: A Decade of Discovery and Diseases. *Immunity* **50**, 1132-1148 (2019).

58. Crotty, S. T follicular helper cell differentiation, function, and roles in disease. *Immunity* **41**, 529-542 (2014).

59. Kim, T.S., Hufford, M.M., Sun, J., Fu, Y.X. & Braciale, T.J. Antigen persistence and the control of local T cell memory by migrant respiratory dendritic cells after acute virus infection. *J Exp Med* **207**, 1161-1172 (2010).

60. GeurtsvanKessel, C.H. *et al.* Dendritic cells are crucial for maintenance of tertiary lymphoid structures in the lung of influenza virus-infected mice. *J Exp Med* **206**, 2339-2349 (2009).

61. Johnston, R.J. *et al.* Bcl6 and Blimp-1 are reciprocal and antagonistic regulators of T follicular helper cell differentiation. *Science* **325**, 1006-1010 (2009).

62. Nurieva, R.I. *et al.* Bcl6 mediates the development of T follicular helper cells. *Science* **325**, 1001-1005 (2009).

63. Hollister, K. *et al.* Insights into the role of Bcl6 in follicular Th cells using a new conditional mutant mouse model. *J Immunol* **191**, 3705-3711 (2013).

64. Rutigliano, J.A. *et al.* Highly pathological influenza A virus infection is associated with augmented expression of PD-1 by functionally compromised virus-specific CD8+ T cells. *J Virol* **88**, 1636-1651 (2014).

65. Tian, Y. & Zajac, A.J. IL-21 and T Cell Differentiation: Consider the Context. *Trends Immunol* **37**, 557-568 (2016).

66. Xin, G. *et al.* A Critical Role of IL-21-Induced BATF in Sustaining CD8-T-Cell-Mediated Chronic Viral Control. *Cell Rep* **13**, 1118-1124 (2015).

67. Liu, X. *et al.* Transcription factor achaete-scute homologue 2 initiates follicular T-helper-cell development. *Nature* **507**, 513-518 (2014).

68. Krishnaswamy, J.K., Alsen, S., Yrlid, U., Eisenbarth, S.C. & Williams, A. Determination of T Follicular Helper Cell Fate by Dendritic Cells. *Front Immunol* **9**, 2169 (2018).

69. Wherry, E.J. & Kurachi, M. Molecular and cellular insights into T cell exhaustion. *Nat Rev Immunol* **15**, 486-499 (2015).

70. Barber, D.L. *et al.* Restoring function in exhausted CD8 T cells during chronic viral infection. *Nature* **439**, 682-687 (2006).

71. Zander, R. *et al.* CD4(+) T Cell Help Is Required for the Formation of a Cytolytic CD8(+) T Cell Subset that Protects against Chronic Infection and Cancer. *Immunity* **51**, 1028-1042 e1024 (2019).

72. Zens, K.D., Chen, J.K. & Farber, D.L. Vaccine-generated lung tissue-resident memory T cells provide heterosubtypic protection to influenza infection. *JCI Insight* **1** (2016).

73. Clemens, E.B., van de Sandt, C., Wong, S.S., Wakim, L.M. & Valkenburg, S.A. Harnessing the Power of T Cells: The Promising Hope for a Universal Influenza Vaccine. *Vaccines (Basel)* **6** (2018).

74. Angeletti, D. & Yewdell, J.W. Is It Possible to Develop a "Universal" Influenza Virus Vaccine? Outflanking Antibody Immunodominance on the Road to Universal Influenza Vaccination. *Cold Spring Harb Perspect Biol* **10** (2018).

75. Estrada, L.D. & Schultz-Cherry, S. Development of a Universal Influenza Vaccine. *J Immunol* **202**, 392-398 (2019).

76. Keeler, S.P. *et al.* Influenza A Virus Infection Causes Chronic Lung Disease Linked to Sites of Active Viral RNA Remnants. *J Immunol* **201**, 2354-2368 (2018).

77. Marchal-Somme, J. *et al.* Cutting edge: nonproliferating mature immune cells form a novel type of organized lymphoid structure in idiopathic pulmonary fibrosis. *J Immunol* **176**, 5735-5739 (2006).

78. Elliot, J.G. *et al.* Aggregations of lymphoid cells in the airways of nonsmokers, smokers, and subjects with asthma. *Am J Respir Crit Care Med* **169**, 712-718 (2004).

79. Yadava, K., Bollyky, P. & Lawson, M.A. The formation and function of tertiary lymphoid follicles in chronic pulmonary inflammation. *Immunology* **149**, 262-269 (2016).

80. Rangel-Moreno, J. *et al.* Inducible bronchus-associated lymphoid tissue (iBALT) in patients with pulmonary complications of rheumatoid arthritis. *J Clin Invest* **116**, 3183-3194 (2006).

81. Hollern, D.P. *et al.* B Cells and T Follicular Helper Cells Mediate Response to Checkpoint Inhibitors in High Mutation Burden Mouse Models of Breast Cancer. *Cell* **179**, 1191-1206 e1121 (2019).

82. Helmink, B.A. *et al.* B cells and tertiary lymphoid structures promote immunotherapy response. *Nature* **577**, 549-555 (2020).

83. Cabrita, R. *et al.* Tertiary lymphoid structures improve immunotherapy and survival in melanoma. *Nature* **577**, 561-565 (2020).

84. Milner, J.J. *et al.* Runx3 programs CD8(+) T cell residency in non-lymphoid tissues and tumours. *Nature* **552**, 253-257 (2017).

85. Zhang, L. *et al.* Lineage tracking reveals dynamic relationships of T cells in colorectal cancer. *Nature* **564**, 268-272 (2018).

86. Steach, H.R. *et al.* Cross-Reactivity with Self-Antigen Tunes the Functional Potential of Naive B Cells Specific for Foreign Antigens. *J Immunol* **204**, 498-509 (2020).

87. Butler, A., Hoffman, P., Smibert, P., Papalexi, E. & Satija, R. Integrating single-cell transcriptomic data across different conditions, technologies, and species. *Nat Biotechnol* **36**, 411-420 (2018).

Figure 1

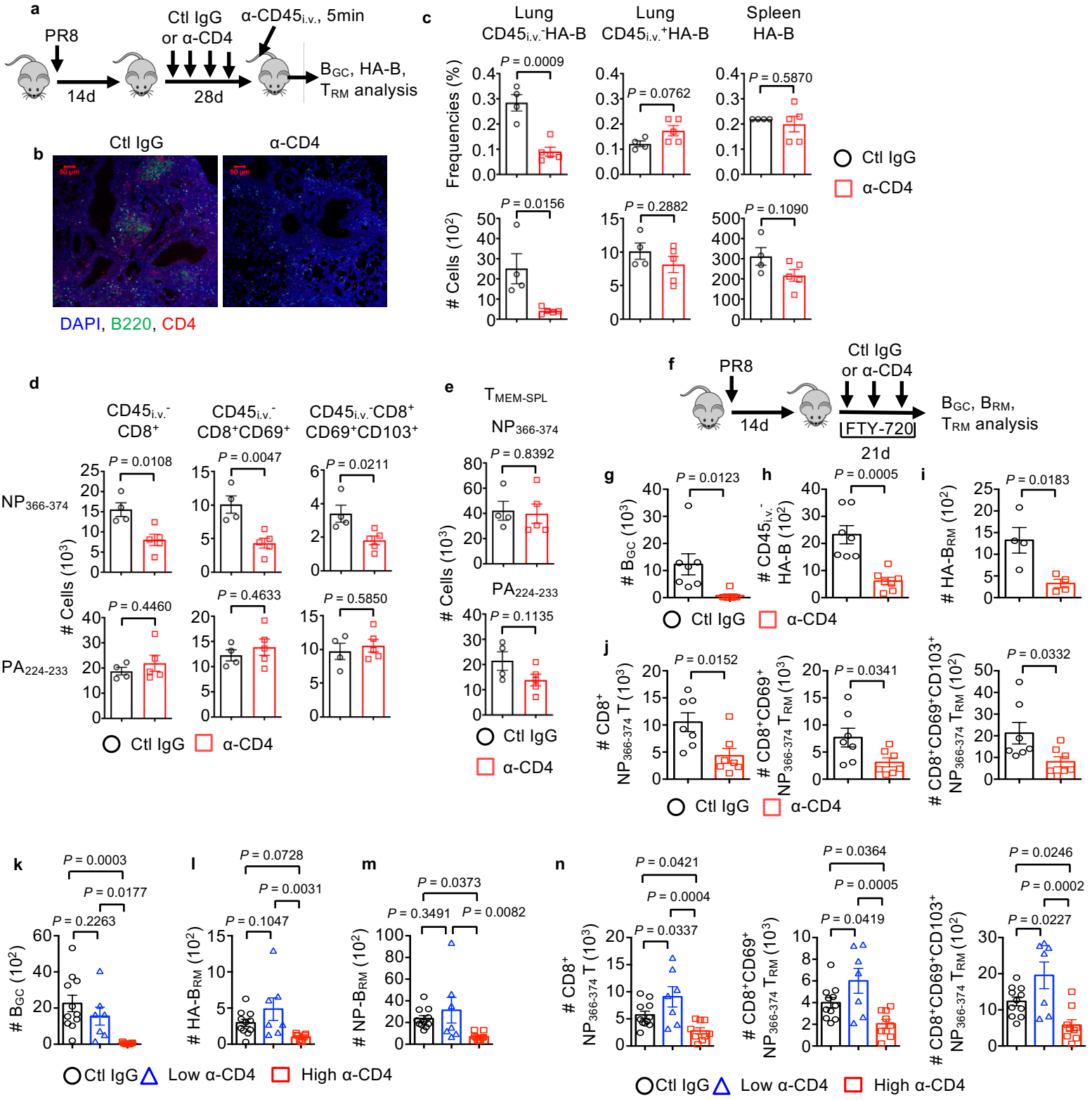

Figure 2

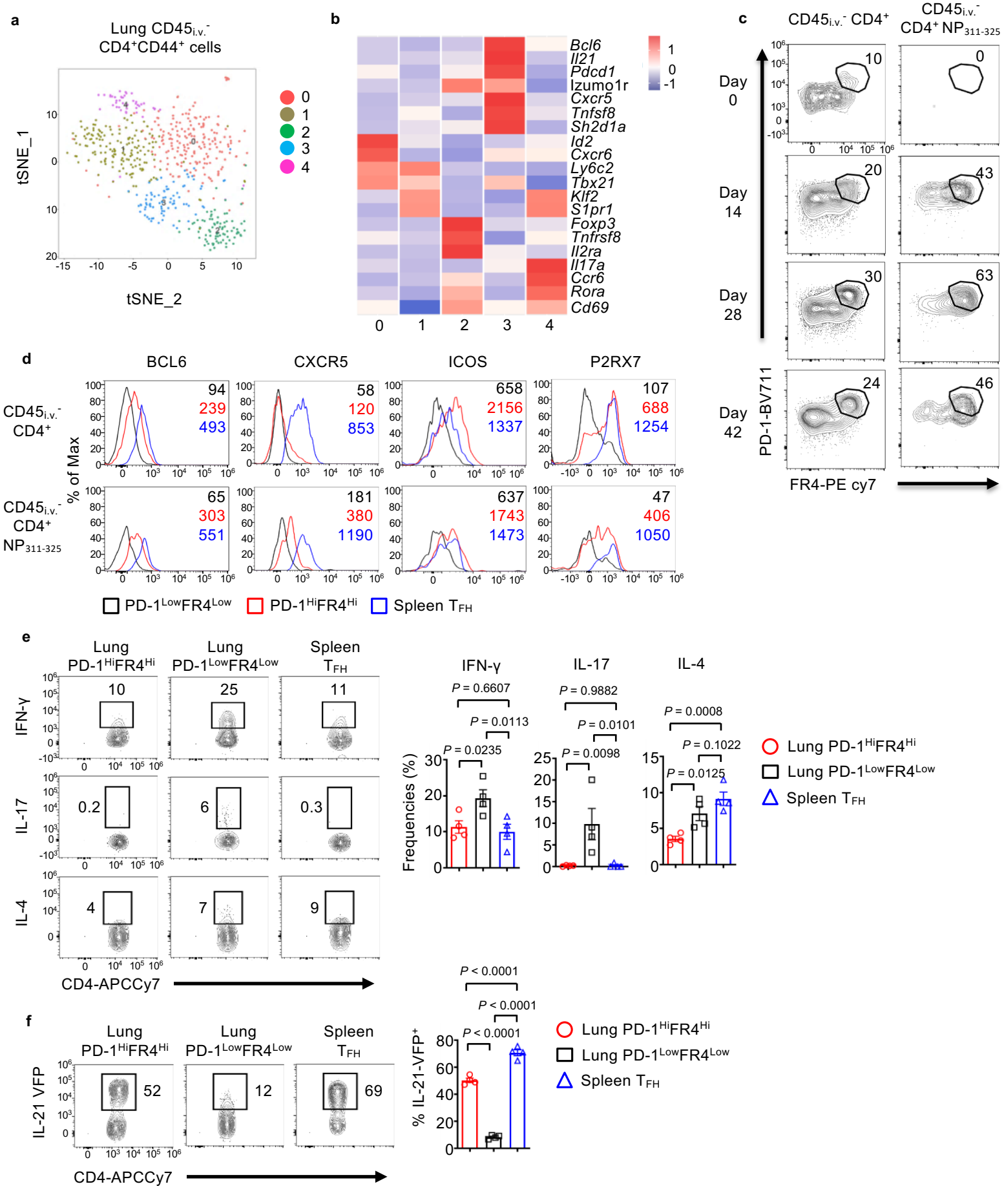

Figure 3

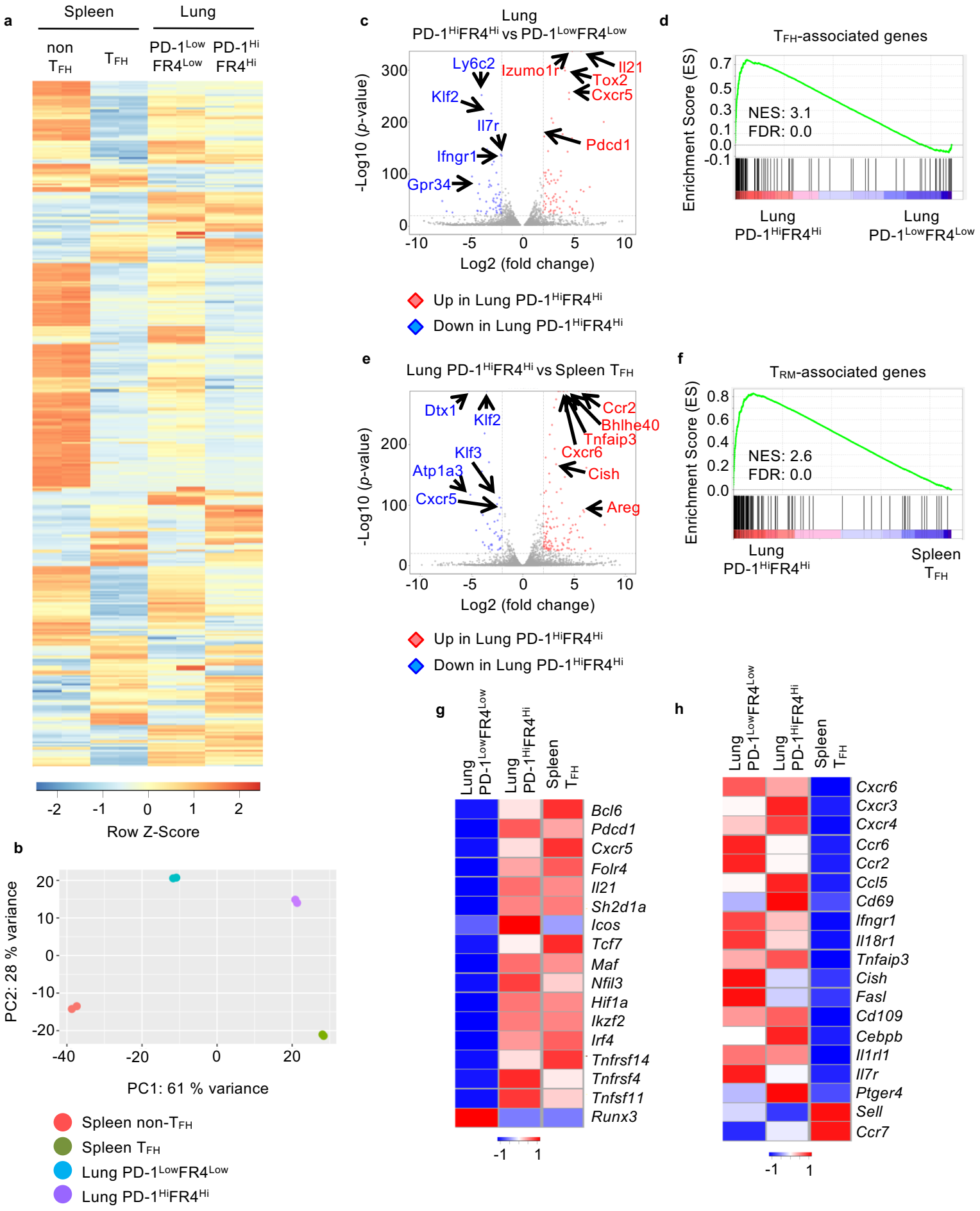

Figure 4

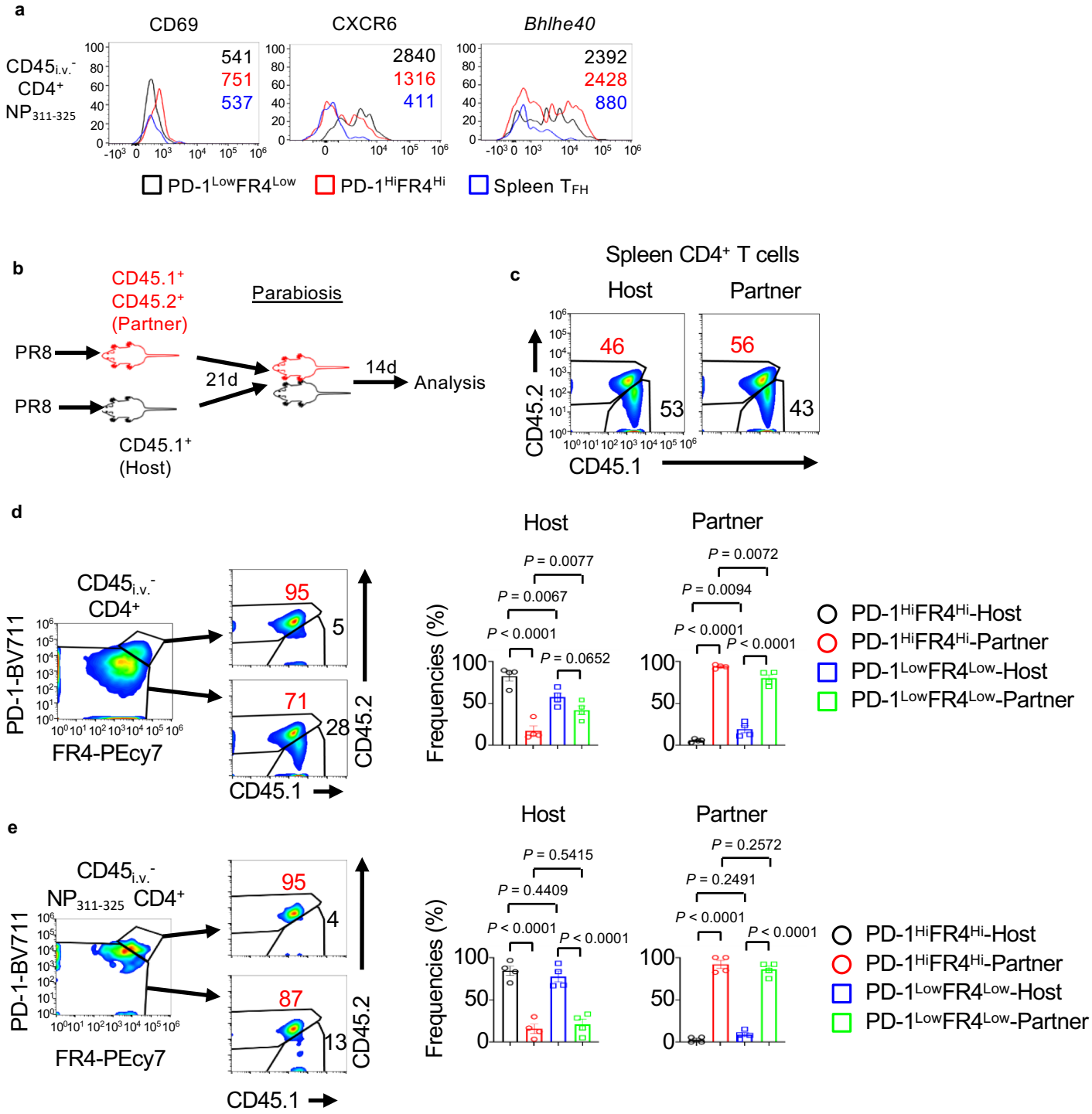

Figure 5

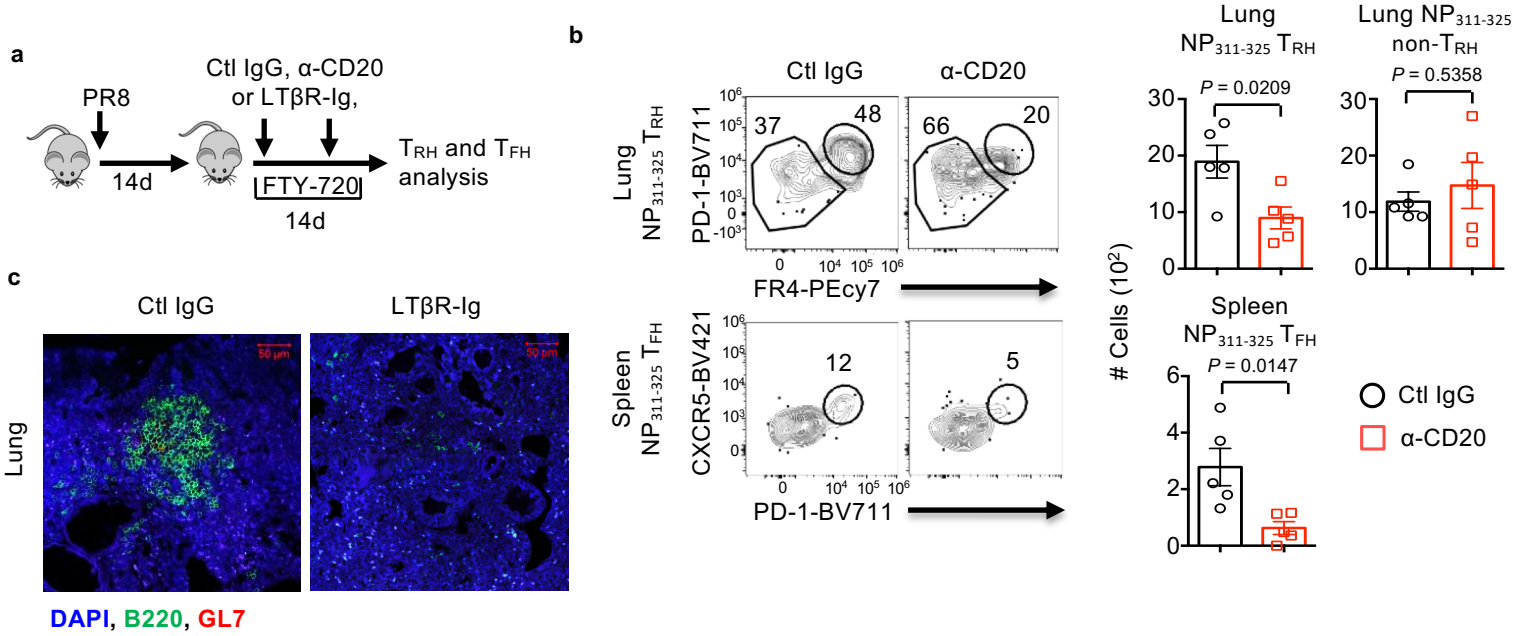

Figure 6

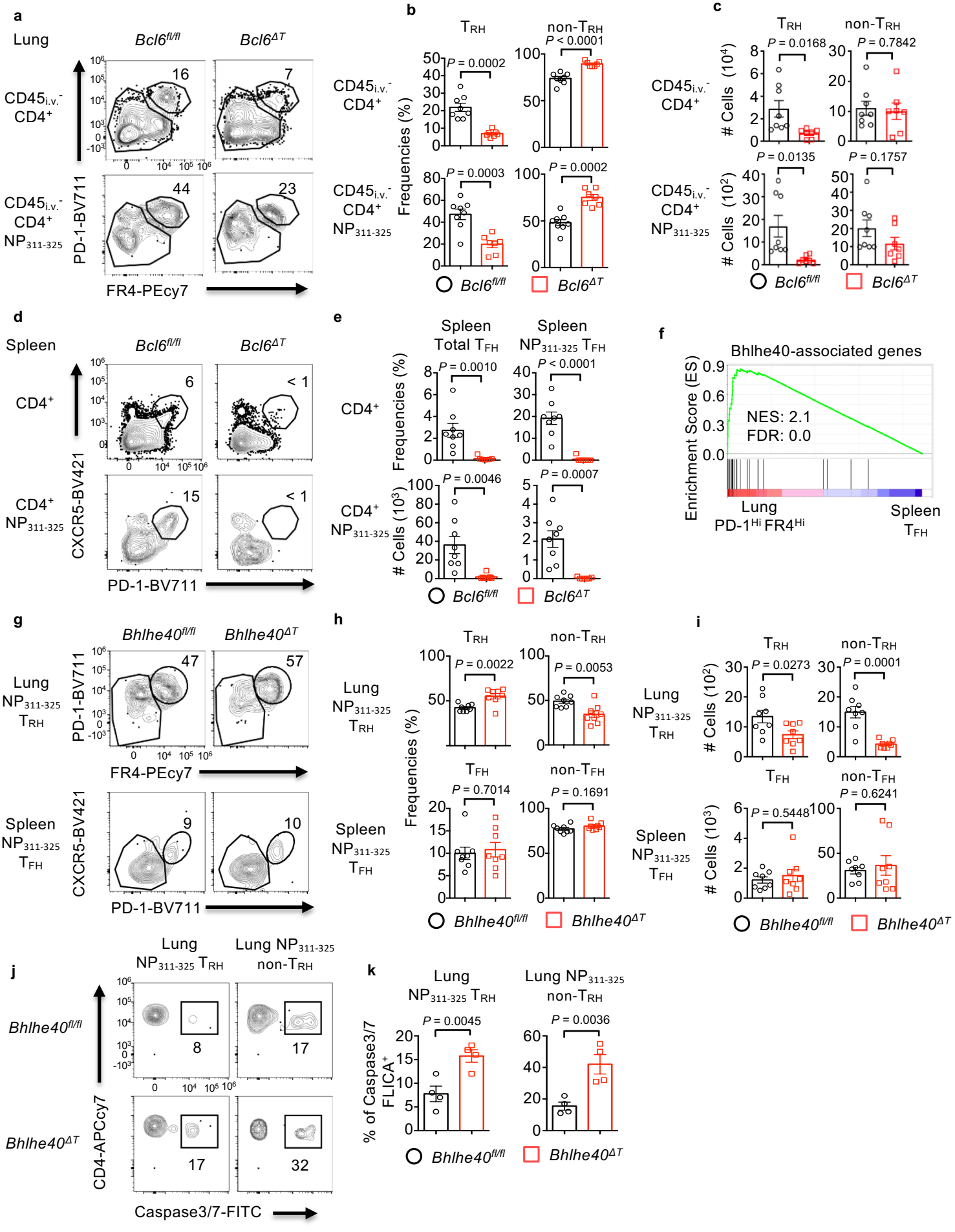

Figure 7

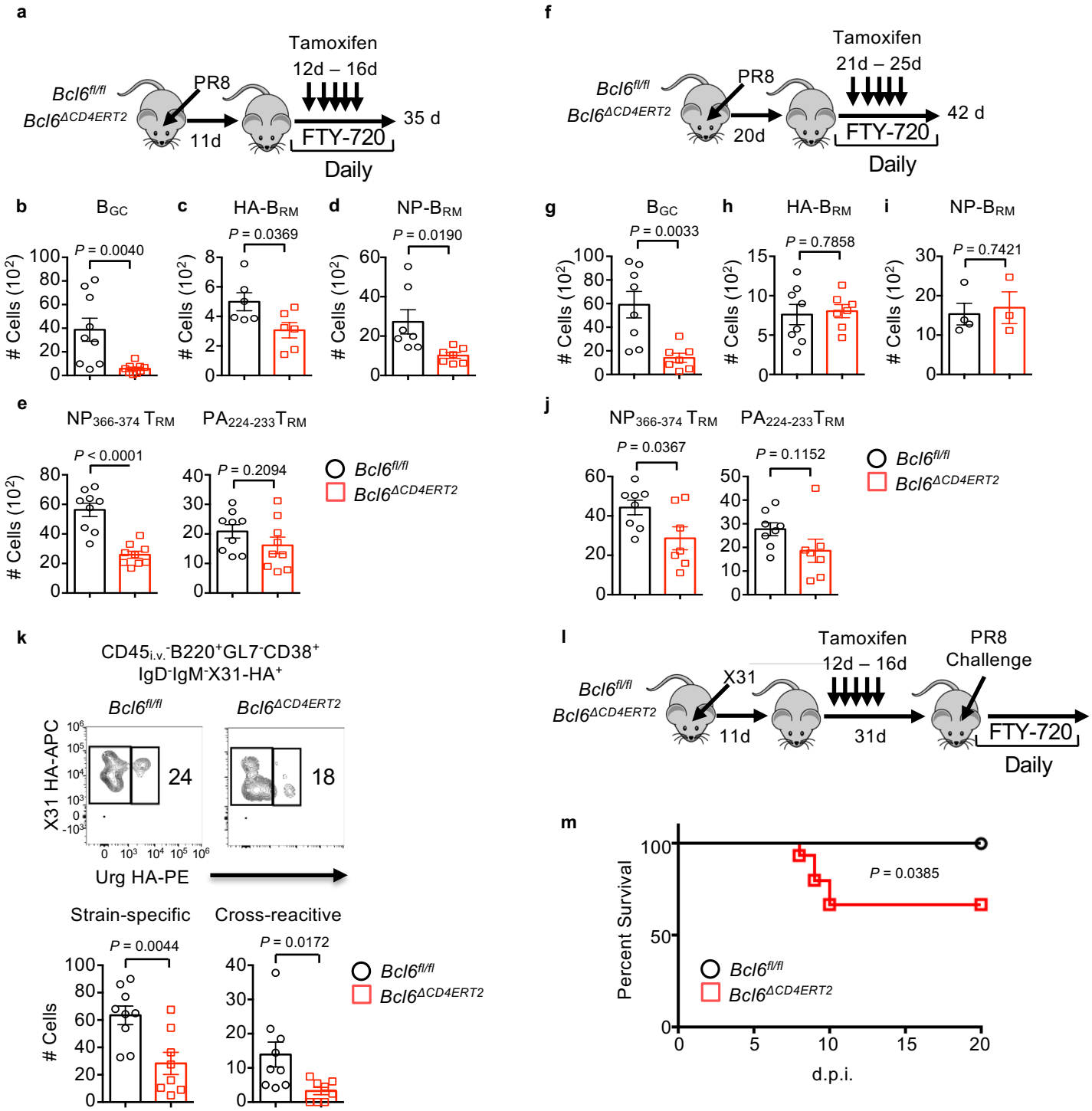

Figure 8

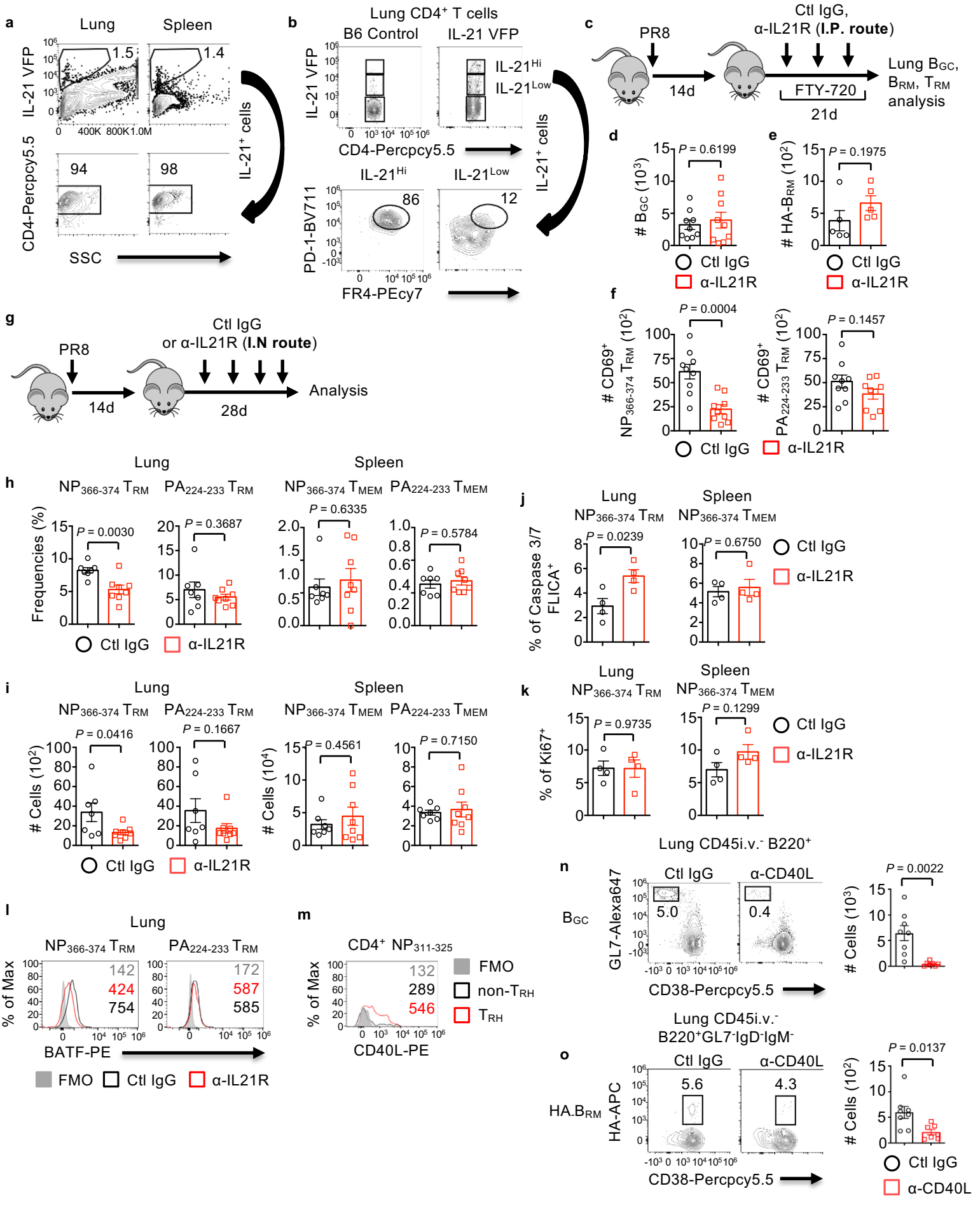

Extended Fig. 1

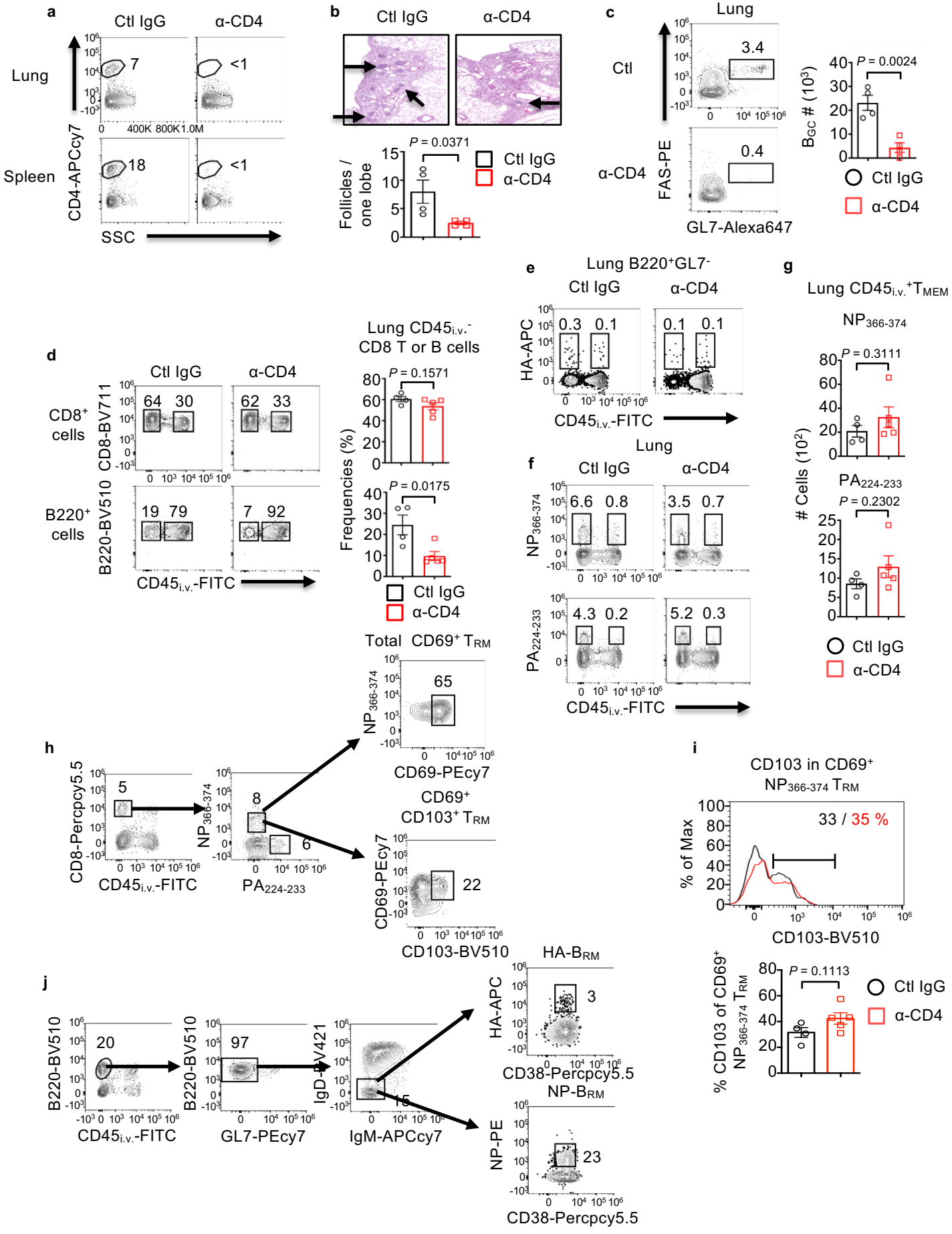

Extended Fig. 2

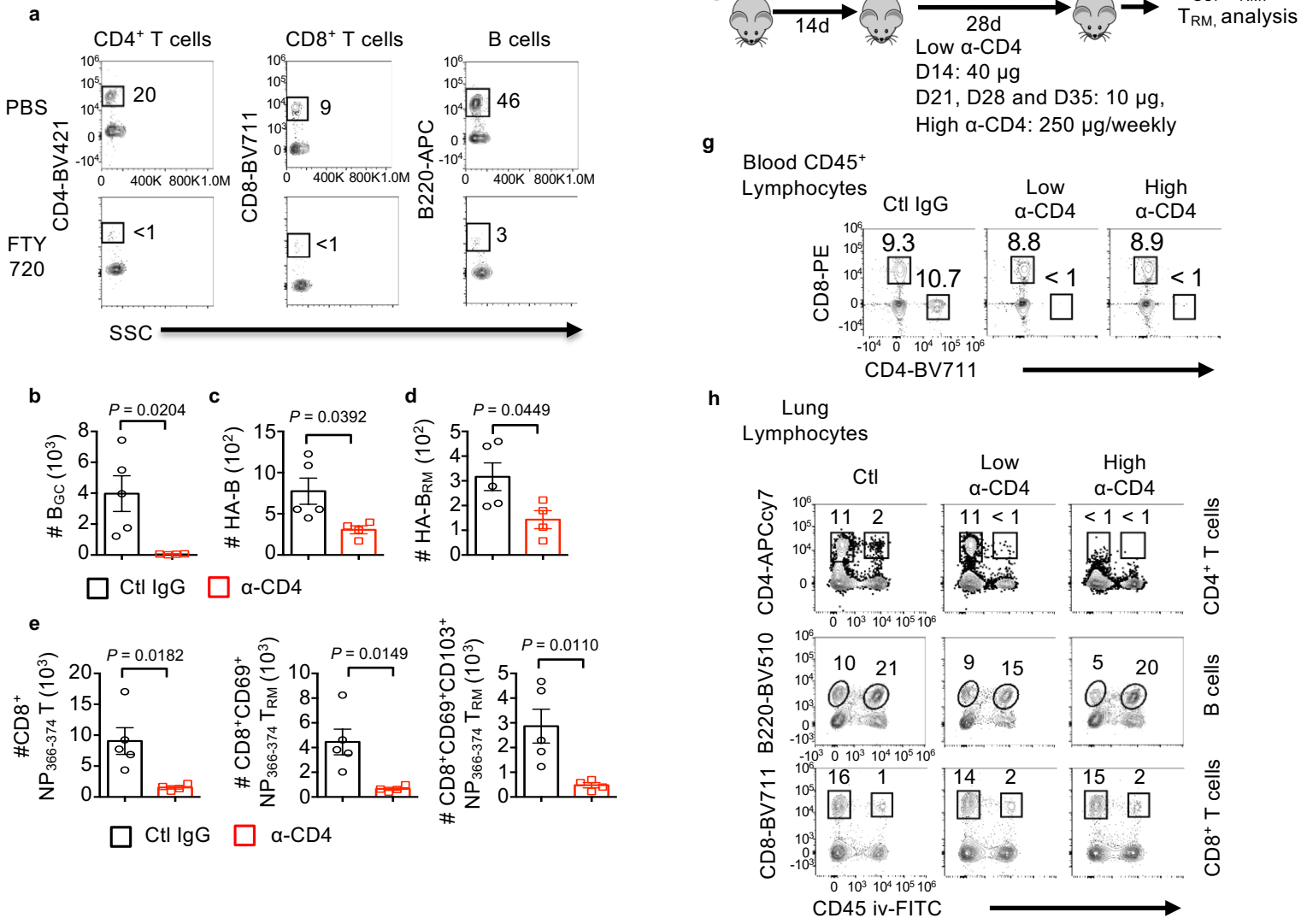

Extended Fig. 3

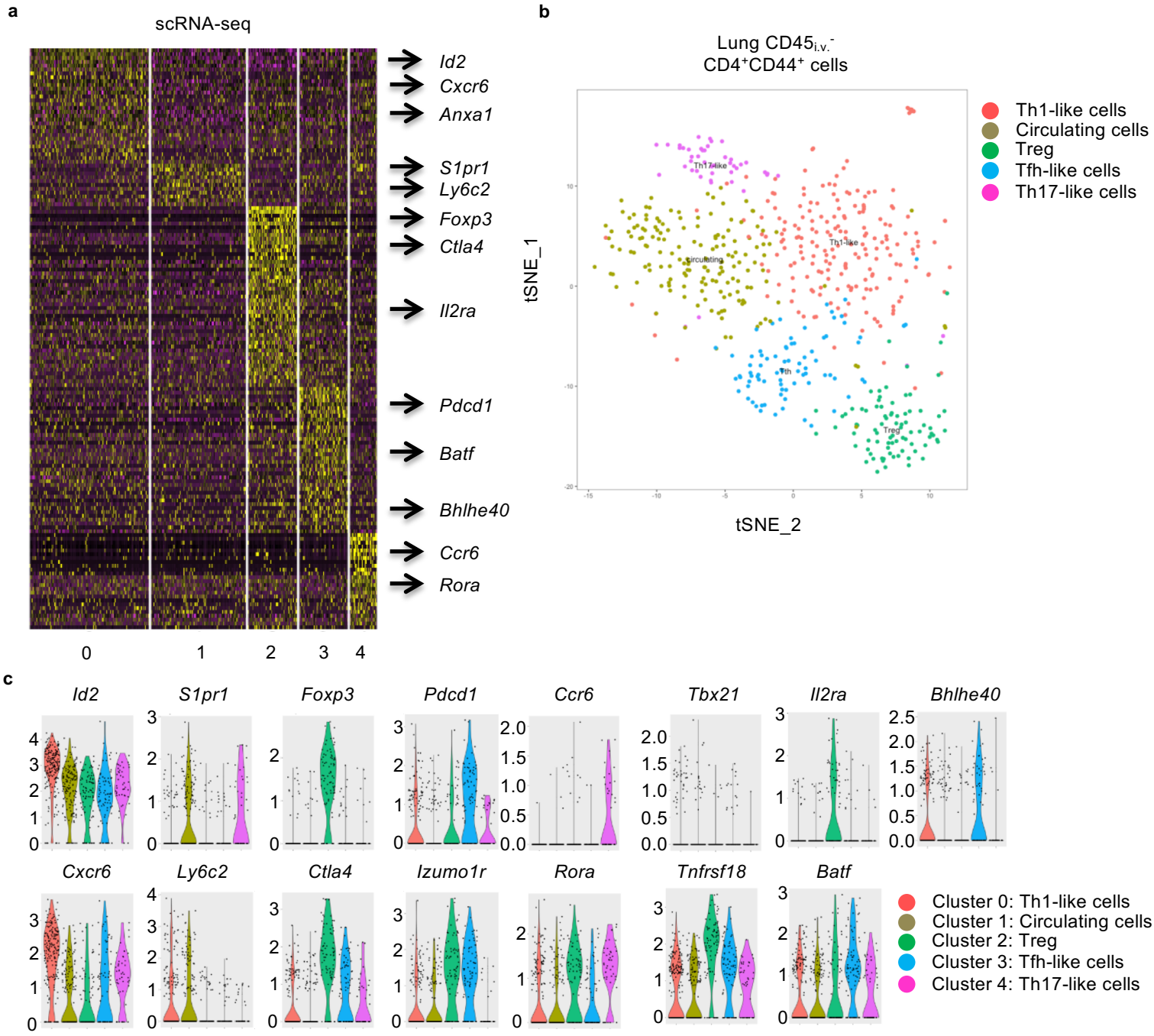

Extended Fig. 4

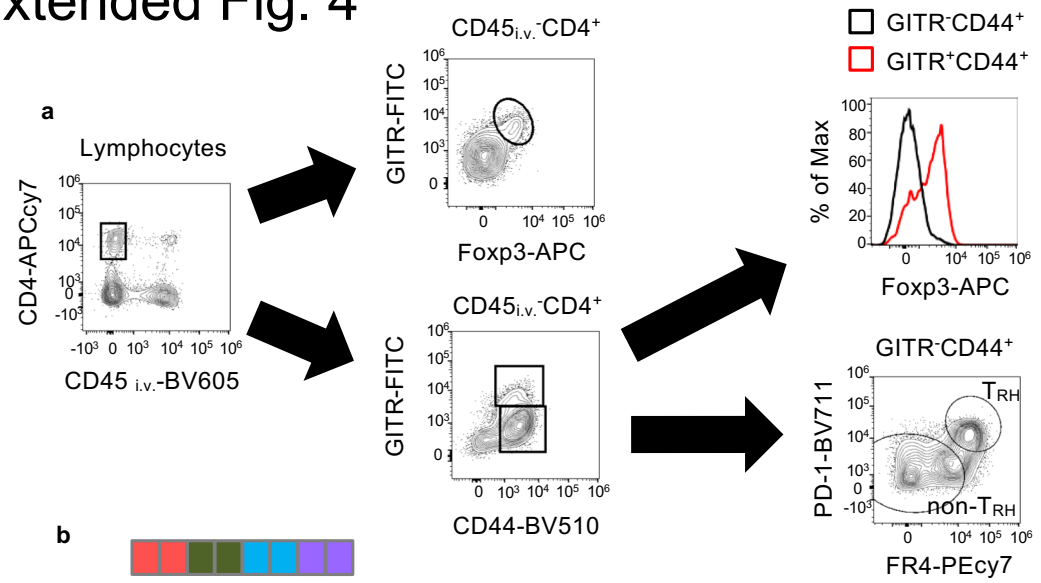

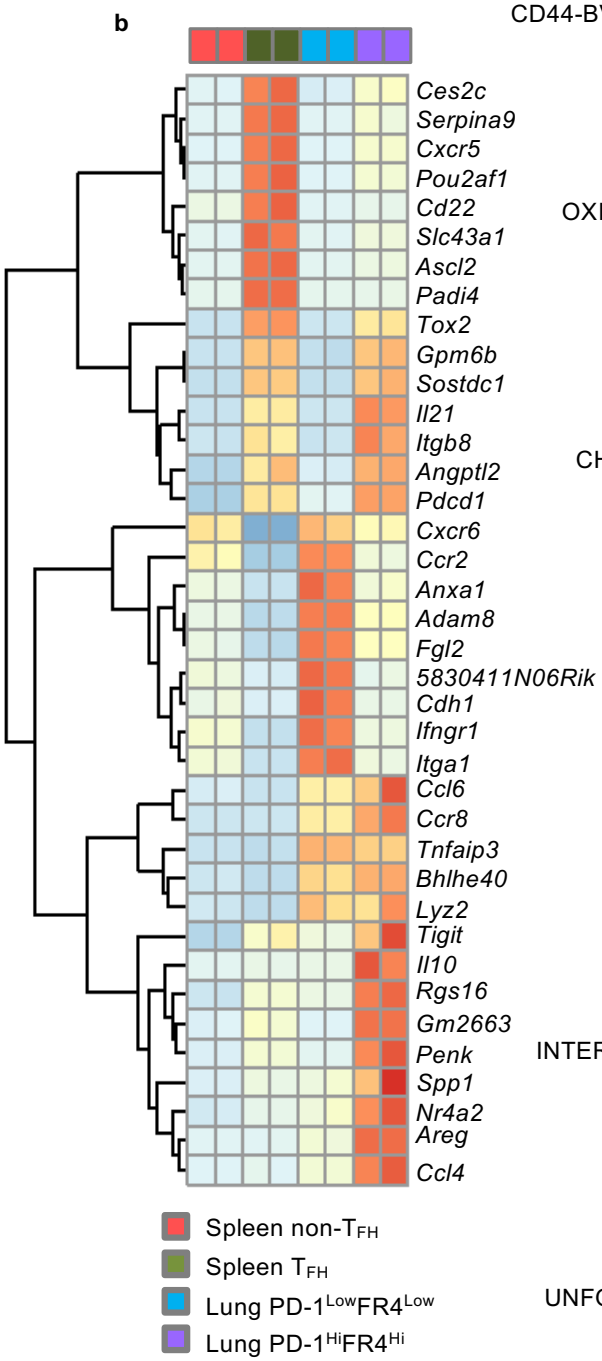

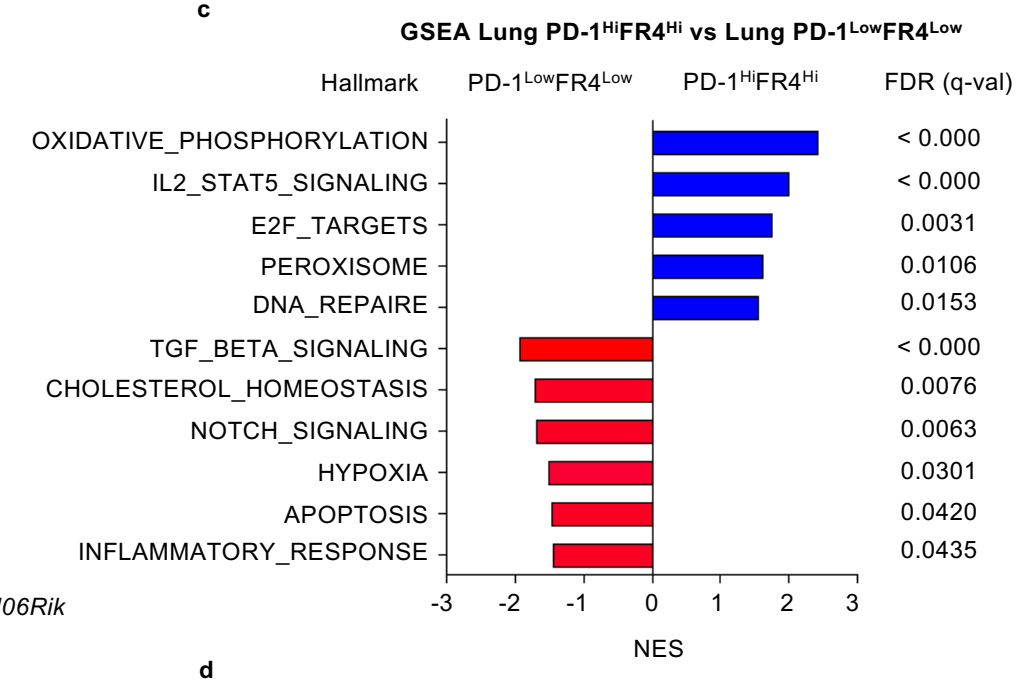

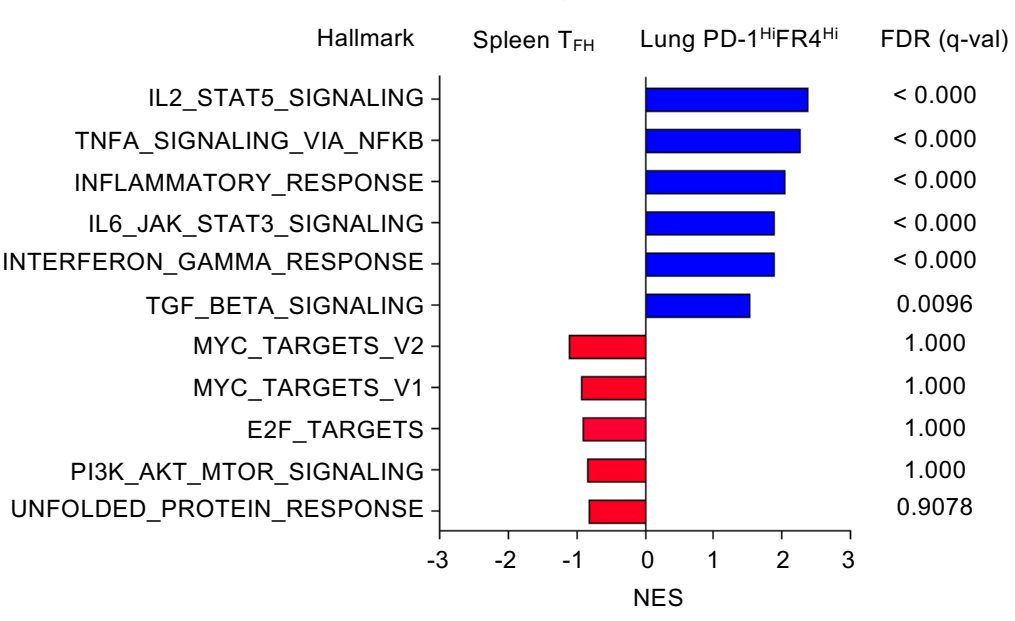

Extended Fig. 5

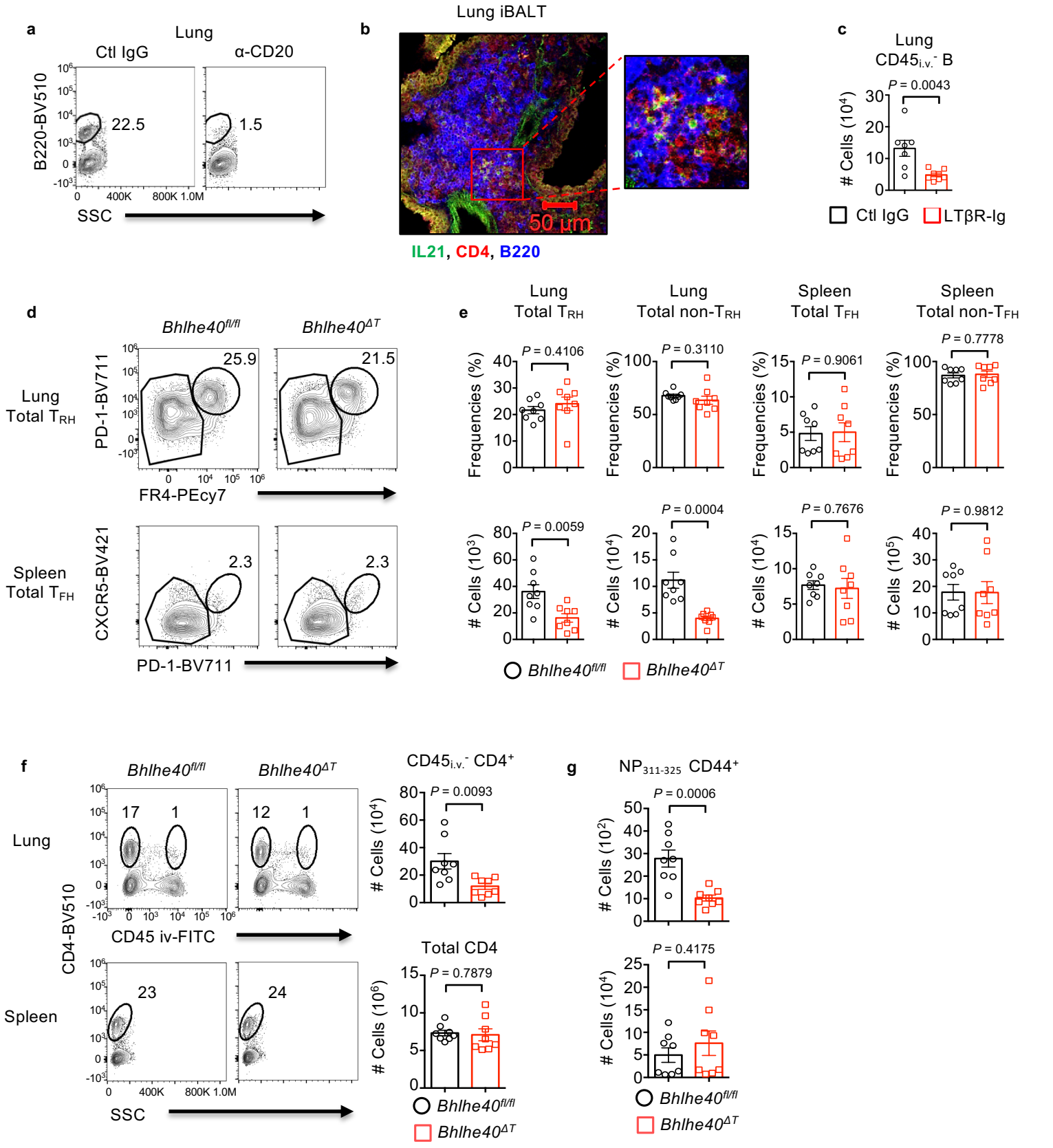

Extended Fig. 6

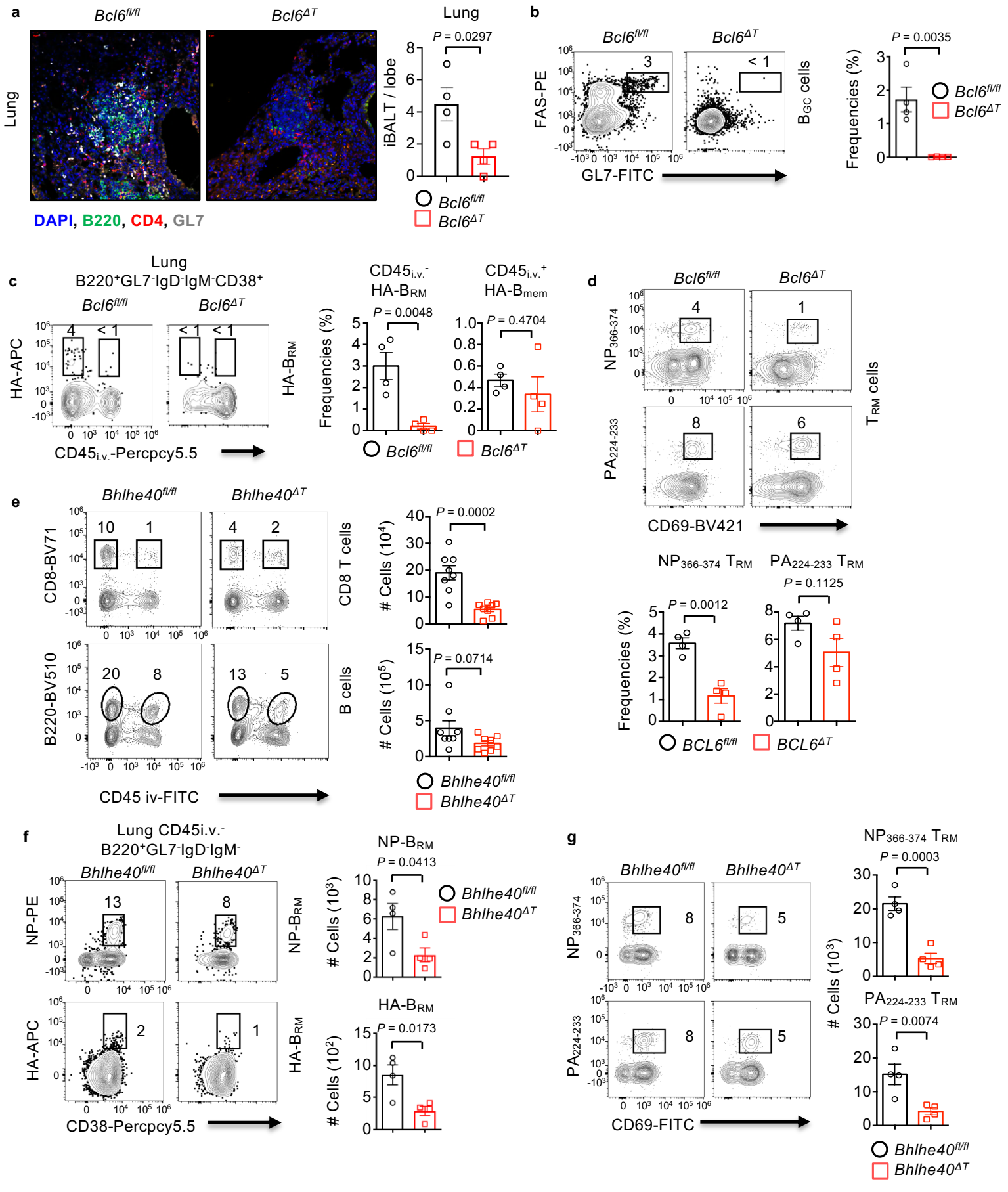

Extended Fig. 7

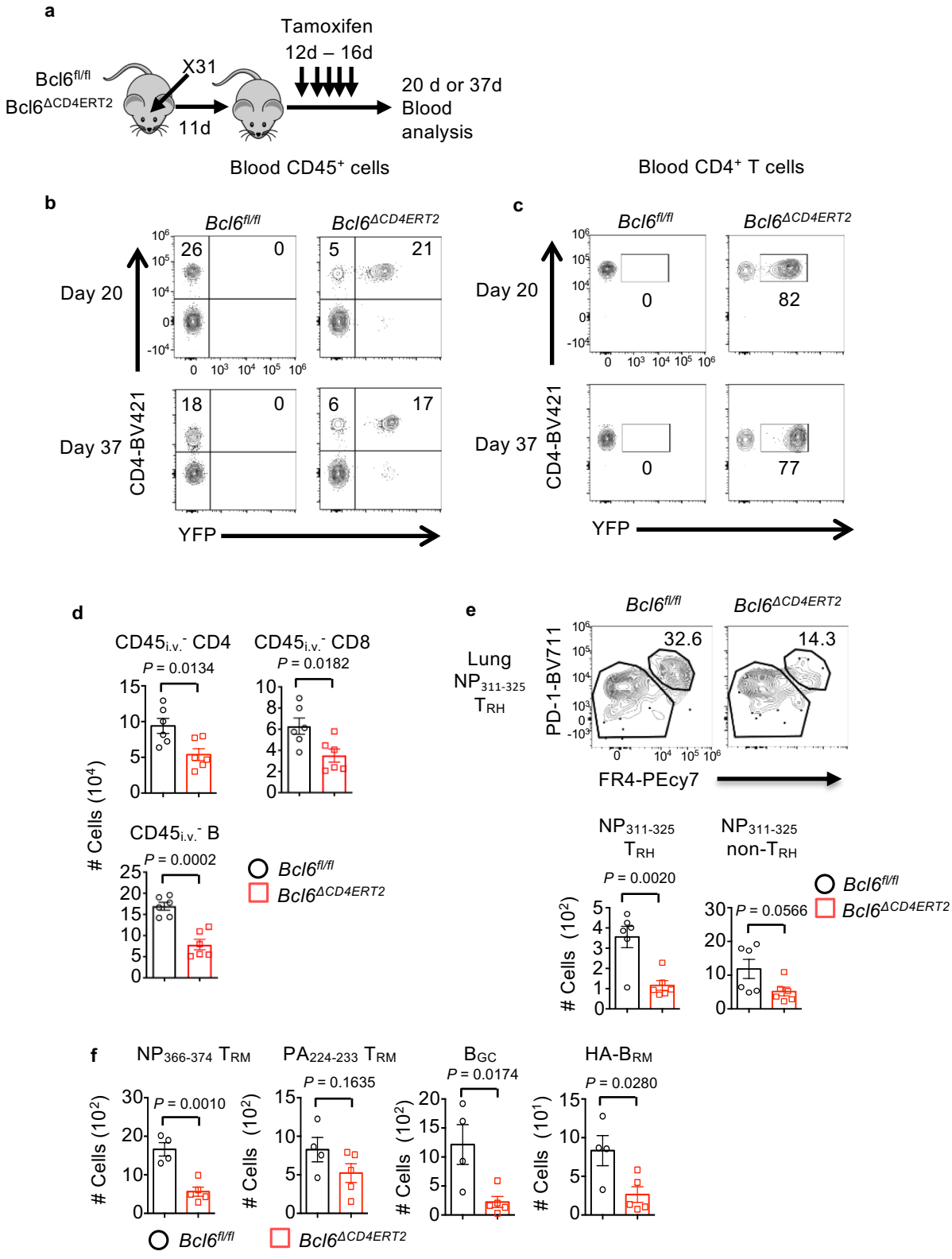

Extended Fig. 8